Check for updates

Received: 15 September 2023 | Revised: 24 December 2023 | Accepted: 2 January 2024

DOI: 10.1111/bre.12845

Basin Research IAS EAGE WILEY

RESEARCH ARTICLE

Integrated uplift, subsidence, erosion and deposition in a tightly coupled source-to-sink system, Pagliara basin, northeastern Sicily, Italy

F. Pavano[1] | F. J. Pazzaglia[1] | T. M. Rittenour[2] | S. Catalano[3] | L. B. Corbett[4] | P. Bierman[4]

[1]Earth and Environmental Sciences Department, Lehigh University, Bethlehem, Pennsylvania, USA

[2]Department of Geology, Utah State University, Logan, Utah, USA

[3]Department of Biological, Geological and Environmental Sciences, Catania University, Catania, Italy

[4]Rubenstein School of the Environment and Natural Resources, University of Vermont, Burlington, Vermont, USA

Correspondence
F. Pavano, Earth and Environmental Sciences Department, Lehigh University, Bethlehem, PA, USA.
Email: frp319@lehigh.edu

Funding information
National Science Foundation, Grant/Award Number: 1904262 and 1735676

Abstract

How tectonic forcing, expressed as base level change, is encoded in the stratigraphic and geomorphic records of coupled source-to-sink systems remains uncertain. Using sedimentological, geochronological and geomorphic approaches, we describe the relationship between transient topographic change and sediment deposition for a low-storage system forced by rapid rock uplift. We present five new luminescence ages and two terrestrial cosmogenic nuclide paleo-erosion rates for the late Pleistocene Pagliara fan-delta complex and we model corresponding base level fall history and erosion of the source catchment located on the Ionian flank of the Peloritani Mountains (NE-Sicily, Italy). The Pagliara delta complex is part of the broader Messina Gravel-and-Sands lithostratigraphic unit that outcrops along the Peloritani coastal belt as extensional basins have been recently inverted by both normal faults and regional uplift at the Messina Straits. The deltas exposed at the mouth of the Pagliara River have constructional tops at ca. 300 m a.s.l. and onlap steeply east-dipping bedrock at the coast to thickness between ca. 100 and 200 m. Five infrared-stimulated luminescence (IRSL) ages collected from the delta range in age from ca. 327 to 208 ka and indicate a vertical long-term sediment accumulation rate as rapid as ca. 2.2 cm/yr during MIS 7. Two cosmogenic ^{10}Be concentrations measured in samples of delta sediment indicate paleo-erosion rates during MIS 8–7 near or slightly higher than the modern rates of ca. 1 mm/yr. Linear inversion of Pagliara fluvial topography indicates an unsteady base level fall history in phase with eustasy that is superimposed on a longer, tectonically driven trend that doubled in rate from ca. 0.95 to 1.8 mm/yr in the past 150 ky. The combination of footwall uplift rate and eustasy determines the accommodation space history to trap the fan-deltas at the Peloritani coast in hanging wall basins, which are now inverted, uplifted and exposed hundreds of metres above the sea level.

This is an open access article under the terms of the Creative Commons Attribution-NonCommercial-NoDerivs License, which permits use and distribution in any medium, provided the original work is properly cited, the use is non-commercial and no modifications or adaptations are made.
© 2024 The Authors. *Basin Research* published by International Association of Sedimentologists and European Association of Geoscientists and Engineers and John Wiley & Sons Ltd.

1 | INTRODUCTION

The geologic inverse problem of reconstructing rock uplift and mountain building from basin stratigraphy goes back at least to Playfair (1802), and interpretations of tectonic processes from sediment texture (reviewed in Blair & Bilodeau, 1988; Matenco & Haq, 2020), provenance (Dickinson & Suczek, 1979) or arrangement of basin facies (Burbank, 1992; Dorsey et al., 1997; Slingerland, 1990) dominates the basin analysis literature (Allen & Allen, 2013; Kim & Paola, 2007; Miall, 1997; Olsen et al., 2018; Paola, 2000; Paola et al., 2001). However, unsteady production of sediment in the source (Bull, 1991; Schumer et al., 2011; Sharman et al., 2019; Smith, 1994; Tucker & Slingerland, 1997), the climatic modulation of base level in the sink (Vail et al., 1977), and variable coupling between tectonics and surface processes that exhibit a range of autogenic behaviours (Beaumont et al., 1992; Hoffman & Grotzinger, 1993; Koons, 1989; Zeitler et al., 2001) obscure the record of tectonic forcing in sediments and sedimentary rocks (Romans et al., 2015; Straub et al., 2009). For example, surface autogenic processes (Feng et al., 2019; Foreman & Straub, 2017), effective diffusivity (Paola et al., 1993), characteristic time scales (Jerolmack & Sadler, 2007) and response times of the system (τ) (Whipple & Tucker, 1999) introduce significant uncertainty in how tectonic processes drive unsteady sediment yield (Jerolmack & Paola, 2010), how they can be interpreted from the architecture of sedimentary basin fill (Allen, 2008), or how they are used to infer the time preserved by sedimentary facies (Paola et al., 2018). Understanding how all of these factors operating on an erosional landscape, ultimately becoming the sedimentary facies in sedimentary basins, is crucial to inversion of the stratigraphic record (Sharman et al., 2019).

Although the response of coupled source-to-sink systems to changes in tectonics are documented in analogue (Bonnet & Crave, 2003; Ganti et al., 2016; Kim & Paola, 2007; Rohais et al., 2012; Trampush et al., 2017) and numeric models (Allen & Densmore, 2000; Armitage et al., 2011; Densmore et al., 2007; Forzoni et al., 2014; Li et al., 2018; Simpson & Castelltort, 2012), large-scale storage in natural systems tends to obscure the encoding of the tectonic forcing in the corresponding stratigraphy (Allen & Densmore, 2000; Castelltort & Van Den Driessche, 2003; Pizzuto et al., 2017; Schumm & Rea, 1995). Here, we capitalize on a natural experiment playing out on a tectonically active Mediterranean plate boundary where unsteady and non-uniform tectonic processes have conspired with glacio-climatic changes in base level and sediment supply to construct a series of marine fan-deltas that can be directly connected to their source basins. The stratigraphy of the deltas, age models that constrain the time of their deposition, their elevation with respect to modern base level, and the fluvial topography of their source catchments all bear on the role that tectonic processes play in both shaping the landscape and constructing the resulting sedimentary archive.

Highlights

- We explore exogenic signal encoding in both geomorphic and stratigraphic records in a delta.
- We reconstructed the base level fall history by fluvial inversion.
- We present a new luminescence-based age model of a Pleistocene delta complex.
- The fluvial landscape recorded high-frequency eustasy-driven oscillations of base level.
- Tectonics drive the general stratigraphy and sedimentology architecture of the delta.

The fan-deltas are exposed on the Ionian flank of the Peloritani Mountains of northeast Sicily, along the Africa-Europe convergent plate boundary (Serpelloni et al., 2007; Figure 1a), one of the most tectonically active regions of the Central Mediterranean (Figure 1b). Specifically, the ca. 30 km^2 Pagliara catchment, centred on the rapidly uplifting footwall of the Taormina normal fault (Figure 1c,d) (Catalano et al., 2008), feeds a series of 100–200 m thick coarse fan-deltas that are part of a constructional coastal plain with the Ionian Sea serving as the base level. Rare, continuous exposure in these deltas in a large gravel quarry operation afford access for reconstructing facies architectures, sampling delta sediments to determine erosion rates during the time of delta aggradation and constructing a geochronologically based age model, all of which we present below. The overall goal of this effort is to make an integrated process model of uplift, subsidence, erosion and sediment yield for a natural setting where the climate and base level changes are well-known (Antonioli et al., 2006; Catalano & De Guidi, 2003; De Guidi et al., 2003; Ferranti et al., 2010; Rust & Kershaw, 2000), sediment storage is minimized, and the response times to tectonic forcing are short (Pavano et al., 2016).

In this paper, we use our findings to explore the relative contributions of tectonics, sediment yield and eustasy in building stratigraphy. We first use our luminescence-constrained age model to describe the deposition and then uplift of the clastic sequence preserved in the footwall of a major normal fault embedded in a deforming forearc. Our data aligns with some recent studies that shows that rates of sediment accumulation are not dependent on changes in the rate of erosion during glacial–interglacial climate change (Ott

13652117, 2024, 1, Downloaded from https://onlinelibrary.wiley.com/doi/10.1111/bre.12845 by Uni Federico II Di Napoli, Wiley Online Library on [17/01/2024]. See the Terms and Conditions (https://onlinelibrary.wiley.com/terms-and-conditions) on Wiley Online Library for rules of use; OA articles are governed by the applicable Creative Commons License

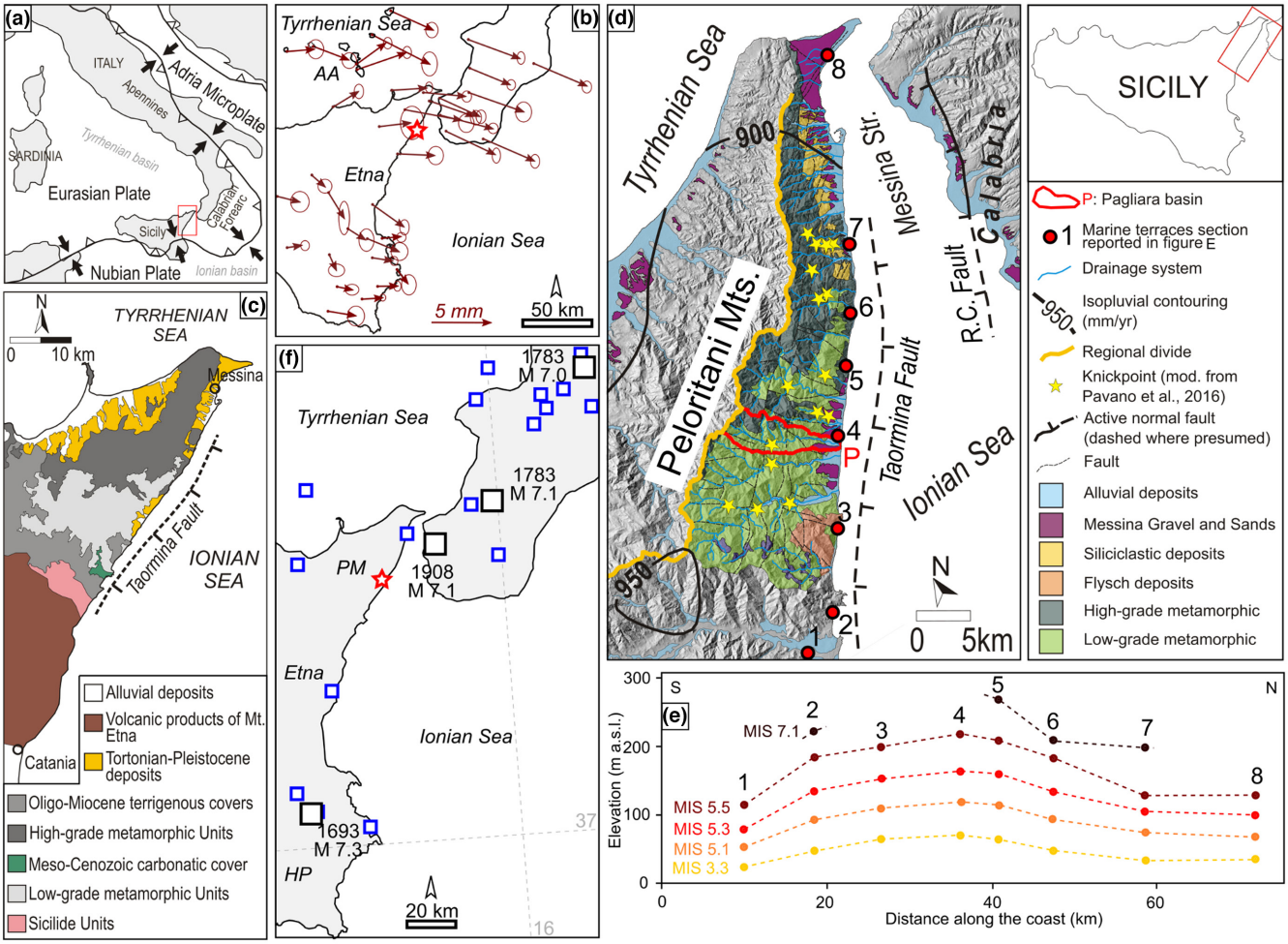

FIGURE 1 (a) sketch map showing the location of Sicily and the Calabrian Forearc in the geodynamic context of the Nubia-Eurasia Plate convergence in the Central Mediterranean area. The red box frames figure (c). (b) GPS vectors referred to Nubia. The red star indicates the location of the Pagliara basin (mod. from Mastrolembo Ventura et al., 2014). (c) Geological setting of northeastern Sicily (mod. from Lentini et al., 1995 and Pavano et al., 2016). (d) Geological-tectonic and morphological settings of the Peloritani Mts. in NE-Sicily where the study area is located (P: Pagliara Basin). Red circles and numbers refer to the location of marine terraces sections reported in figure (e). (e) distribution, along the coast, of the elevation of marine terraces' inner edges (mod. from Catalano & De Guidi, 2003). MIS: Marine Isotope Stage. (f) distribution of large historic earthquakes in eastern Sicily and southern Calabria, where large black boxes indicate Mw>7 events, whereas smaller blue boxes indicate 5<Mw<7 events (Rovida et al., 2022).

et al., 2022). The age model allows us to then integrate the sedimentologic data with an inversion of the fluvial topography (Gallen, 2018; Goren et al., 2014; Pavano & Gallen, 2021; Pazzaglia & Fisher, 2022) that links uplift and erosion in the source to subsidence and deposition in the sink, and the construction of the sedimentary architecture of the Pagliara delta complex.

2 | SETTING

The Peloritani Mountains compose the northeastern tip of Sicily, which is embedded in the actively translating Calabrian Forearc, marking the subduction of Nubian plate beneath Eurasian plate in the central Mediterranean (Amodio Morelli et al., 1976; Dewey et al., 1989; Malinverno & Ryan, 1986) (Figure 1a). The forearc is an orocline made up of crystalline basement with Europe-affinity (Catalano et al., 2018; Lentini & Vezzani, 1975; Pezzino et al., 2008) that separated from Sardinia ca. 6 Ma (Malinverno, 2012). Southeast-directed translation of the forearc (Figure 1b), presumably by Ionian slab rollback, led to the Sicilian collision and the opening of the Tyrrhenian basin (Boccaletti et al., 1990; Faccenna et al., 2004, 2011; Kastens et al., 1988; Rosenbaum & Lister, 2004). The Peloritani Mountains are underlain by stacked tectonic-metamorphic units consisting of juxtaposed, top-to-bottom, high-grade and medium-to-low-grade Hercynian European-affinity crystalline basement (Catalano et al., 2018; Lentini et al., 2000; Lentini

13652117, 2024, 1, Downloaded from https://onlinelibrary.wiley.com/doi/10.1111/bre.12845 by Uni Federico II Di Napoli, Wiley Online Library on [17/01/2024]. See the Terms and Conditions (https://onlinelibrary.wiley.com/terms-and-conditions) on Wiley Online Library for rules of use; OA articles are governed by the applicable Creative Commons License

& Vezzani, 1975) (Figure 1c,d). This metamorphic backbone is encircled by late Miocene to late Pleistocene sedimentary rocks deposited within basins controlled by normal fault systems, often arranged in an én-echelon geometry (Lentini et al., 1995; Lentini & Vezzani, 1975).

The Peloritani Mountains are an example of middle to late Pleistocene fragmentation of the forearc by high-angle normal faults (Billi et al., 2006; Cammarata et al., 2018; Foti et al., 2023; Meschis et al., 2018; Pavano et al., 2015). The highest rates of rock uplift, inferred from a marine oxygen isotope stage (MIS) eustatic-based age model of mid-late Pleistocene marine terraces (Figure 1e) and fan-delta deposits (Bada et al., 1991; Bonfiglio, 1983; Catalano et al., 2003), characterize the footwall block of the Taormina fault, that is widely considered to bound the Ionian flank of the range (Antonioli et al., 2006; Catalano et al., 2003, 2008; Catalano & De Guidi, 2003; De Guidi et al., 2003; Pavano et al., 2016). However, the precise structures and kinematics that control this part of the forearc are still debated (Argnani et al., 2009; Barreca et al., 2019; Catalano et al., 2003, 2008; De Guidi et al., 2002; Meschis et al., 2019; Pavano & Gallen, 2021). In this paper, we consider the Taormina normal fault as the northeast Sicily segment of a larger NNE–SSW to NNW–SSE-trending, extensional belt (Catalano et al., 2008; Monaco & Tortorici, 2000) that accommodates continued stretching of the upper plate during SE-directed translation of the forearc.

Down-valley interfluves of major streams draining the Peloritani Mountains to the Ionian Sea host marine terraces (Figure 1e) and are mantled by perched coastal and nearshore clastic deposits. Locally, as is the case for the mouth of the Pagliara drainage, these terraces are inset into ca. 200 m thick fan-deltas (Figure 1d,e; Catalano & De Guidi, 2003) that are part of a broader lithostratigraphic package called the Messina Gravels and Sands (MGS). The fan-deltas at the mouth of the Pagliara accumulated in a now-inverted hanging wall basin of the Taormina fault.

All of northeastern Sicily and southern Calabria is seismically active (Figure 1f), characterized by high-magnitude, catastrophic earthquakes (Boschi et al., 1997; Postpischl, 1985) such as the A.D. 1908 Messina Strait earthquake ($M = 7.1$) (Baratta, 1910; Meschis et al., 2019) (Figure 1f), as well as more frequent medium-magnitude earthquakes (e.g. Azzaro et al., 2007; Cammarata et al., 2018; Giammanco et al., 2008; Scarfì et al., 2016). The lack of a large historic earthquake in the Peloritani Mountains have led some researchers to consider the Taormina fault or related structures as part of a modern seismic gap (Neri et al., 2006). Nevertheless, strong earthquakes including the A.D. 1693 southeastern Sicily earthquake, the 1783 Calabrian earthquakes (Boschi et al., 1997) and the 1908 Messina Strait earthquake (Cello et al., 1982), impacted eastern Sicily and the study area with landslides and tsunami (Baratta, 1910; Comerci et al., 2015; Tinti et al., 2004), even though the precise source of these earthquakes is still debated (Amoruso et al., 2002; Riuscetti & Shick, 1975; Valensise & Pantosti, 1992).

2.1 | MGS deposits

The fan-deltas at the mouth of the Pagliara catchment (Figure 2a) are part of a more widespread middle Pleistocene lithostratigraphic unit up to 250 m thick (MGS) (Bada et al., 1991; Bonfiglio, 1991; Bonfiglio & Violanti, 1984; Lentini et al., 2000; Selli, 1978). These deposits are also known to exist in the Straits of Messina (Del Ben et al., 1996). In general, these deposits consist of gravel and grey-yellowish or reddish-coloured sands, with local shell-rich horizons (Figure 2b). The MGS range from nested prograding fluvio-deltaic bodies, generally organized in foresets and showing channelized fluvial deposits (Figure 2c), to middle-shelf sand waves (Barrier, 1987) (Figure 2d), locally trough cross-stratified (Figure 2e). The former was sourced from small, but steep catchments incised into uplifting footwalls such as the Peloritani Mountains. The latter consists of marine grey sands with large encrusted (*bryozoan, serpulids*; Bonfiglio & Violanti, 1984) pebbles of metamorphic rocks within a poorly stratified sandy matrix. This facies transitions upwards into cemented greyish, stratified sand, containing rounded pebbles from both crystalline and sedimentary terms (Bonfiglio & Violanti, 1984). A middle Pleistocene mammalian fauna (ca. 365–200 ka) has been described from the upper facies (Bada et al., 1991; Bonfiglio, 1991). Collectively, these facies may represent the confluence of several source areas and axial fluvial and marine filling of a now partially inverted Sicily-Calabria extensional belt basin. Sandy marine terraces that unconformably overlie the MGS contain *Strombus bubonius LMK*, a marine gastropod known to be well associated with the MIS 5e eustatic high stand at 125 ka (Bonfiglio & Violanti, 1984).

Locally along the Ionian side of the Peloritani Mts., the MGS is underlain by a polymictic, clast- and matrix-supported, sandy conglomerate, called the Allume Conglomerates (Carbone et al., 2008; Lentini et al., 2000). These deposits are reddish in colour, contain angular to rounded crystalline clasts, onlap the crystalline basement and are bound by high-angle faults in small, disarticulated extensional basins. The MGS unconformably overlie the

13652117, 2024, 1, Downloaded from https://onlinelibrary.wiley.com/doi/10.1111/bre.12845 by Uni Federico II Di Napoli, Wiley Online Library on [17/01/2024]. See the Terms and Conditions (https://onlinelibrary.wiley.com/terms-and-conditions) on Wiley Online Library for rules of use; OA articles are governed by the applicable Creative Commons License

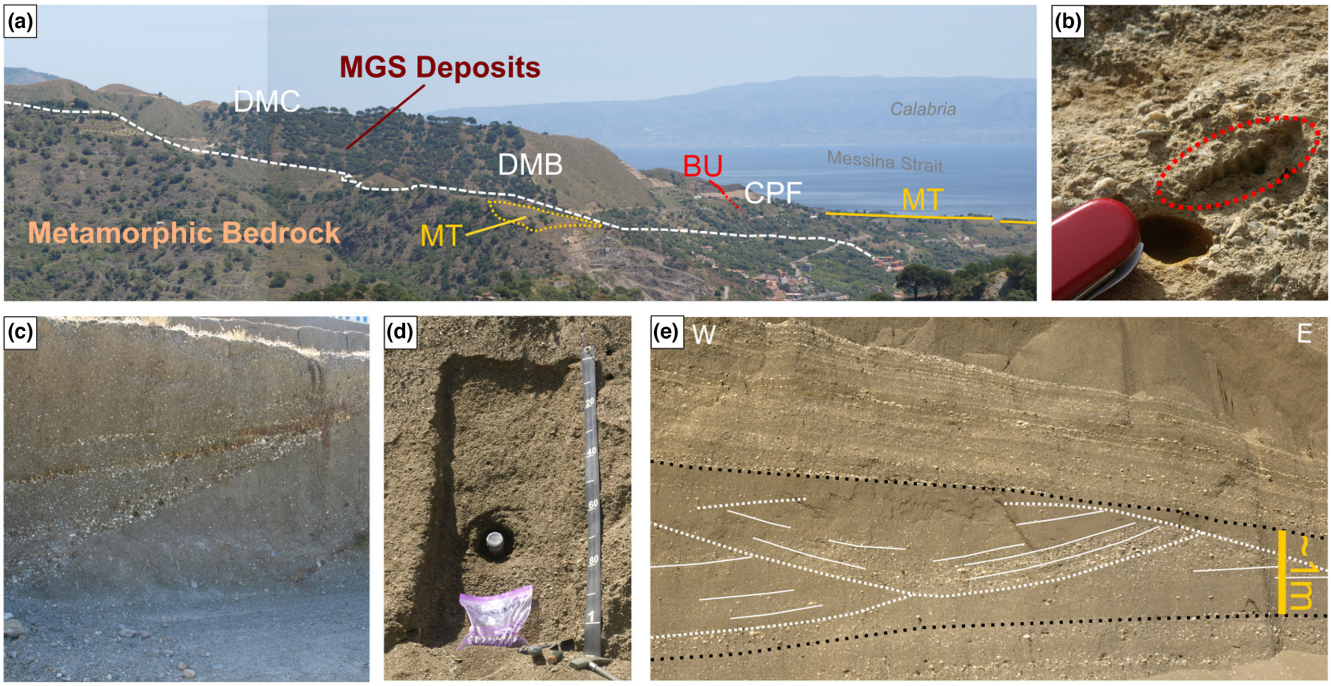

FIGURE 2 (a) panoramic view of the studied Pagliara delta complex depositional sequence of the MGS, lying on a metamorphic bedrock. DMC: Distributary Mouth Channel facies; DMB: Distributary Mouth Bar facies; CPF: Fluvial/Coatal Plain facies; BU: Buttress Unconformity. The location of some of the marine terraced surfaces (MT) are noted. (b) Pecten sp shell indicating marine depositional environment, specifically reported along maximum flooding surface (part of the field knife is for scale). (c) Channelized fluvial deposits unconformably onlapping DMB deposits. (d) Sands and fine gravels horizon within the DMB selected for luminescence sampling site. (e) Detail of a horizon within the DMB deposits showing trough cross-stratification with chute-and-pool structures and lenses of clustered coarser sediments. The different coloured lines highlight the tractive structures. The unannotated version of the field photos is reported in SI 3.

Allume Conglomerates and pre-date the basin-bounding normal faults.

3 | METHODOLOGY

3.1 | Field descriptions

In the study area, the MGS fluvial-deltaic facies are exposed in the O.R. Di Grasso Rosetta e C. S.a.s. quarry near the mouth of the Pagliara River. We made field descriptions of sediment texture, structure and bedding thickness with close attention to unconformities. Following standard approaches for facies descriptions (reviewed in Allen & Allen, 2013) and sequence stratigraphy (reviewed in Catuneanu et al., 2009) the observations are designed to construct the overall stratigraphic architecture of Gilbert-type deltas.

Regarding the facies analysis, water depths of −5 to 10 m are used for distributary mouth channel and bar facies, respectively (Dalrymple et al., 2003). Prodelta facies are considered to have been deposited in water depths ca. 100–200 m. Conversely, fluvial facies are considered to have been deposited from 0 to 10 m.

3.2 | Luminescence geochronology

Our geochronologic age model is assembled from five infrared-stimulated luminescence (IRSL) dating of sand fraction feldspar. IRSL samples targeted beds of diverse facies in the fan-delta deposit that, given their transport through the drainage system, we assume were most likely to have been reset (zeroed) by sunlight prior to the deposition (Nelson et al., 2015; Rittenour, 2018). Sampling followed the USU Luminescence Lab guide (e.g. Nelson et al., 2015, 2019). The samples were opened and processed under dim amber safelight conditions at the Utah State University (USU) Luminescence Lab. Sample processing for IRSL dating followed standard procedures include sieving, HCl and bleach treatments, and heavy mineral separation at 2.58 g/cm^3, with no HF pre-treatment, to isolate the potassium-rich feldspar component of a narrow grain size range of 150–250 μm.

Samples were dated following single-aliquot regenerative-dose procedures (Wallinga et al., 2000). IRSL stimulation was conducted at 50°C over 100 s on a Risø TL/OSL Model DA-20 reader using IR emitting diodes (875 nm) and signal detection through Schott BG-39 and Corning 7–59 filters (320–450 nm). Equivalent

13652117, 2024, 1, Downloaded from https://onlinelibrary.wiley.com/doi/10.1111/bre.12845 by Uni Federico II Di Napoli, Wiley Online Library on [17/01/2024]. See the Terms and Conditions (https://onlinelibrary.wiley.com/terms-and-conditions) on Wiley Online Library for rules of use; OA articles are governed by the applicable Creative Commons License

dose (D_E) values for each aliquot were corrected for anomalous fading (loss of signal overtime) following the methods of Lamothe et al. (2003). Fading rate *g*-values, were normalized to two days of decay and reported as %/decade. IRSL ages are calculated by dividing the fading-corrected D_E (Gy) by the environmental dose rate (Gy/kyr).

Dose rate calculations were determined by chemical analysis of the U, Th, K and Rb content using ICP-MS and ICP-AES techniques and conversion factors from Guérin et al. (2011) (see SI 1). Internal grain beta dose rate was determined assuming 12.5% K (Huntley & Baril, 1997) and 400 ppm Rb (Huntley & Hancock, 2001) attenuated to grain size using Mejdahl (1979). Alpha contribution to dose rate was determined using an efficiency factor, '*a*-value', of 0.15 ± 0.05 after Balescu and Lamothe (1994) (Durcan et al., 2015). The contribution of cosmic radiation to the dose rate was calculated using sample depth, elevation and latitude/longitude following Prescott and Hutton (1994). Dose rates are calculated based on water content, sediment chemistry and cosmic contribution (Aitken, 1998; Aitken & Xie, 1990). See Supplementary Information for supporting dose rate data.

3.3 | Cosmogenic nuclide paleo-erosion rates

Two samples shielded by more than 10 m and co-located with IRSL ages were collected from deltaic and fluvial facies, respectively, to determine the concentration of in situ cosmogenic ^{10}Be in quartz. Knowing the burial age of the sample and the half-life of ^{10}Be, the ^{10}Be concentration can be used to determine the steady-state exposure erosion rate of the sediment at the time when it was received from the catchment. We assume simple rapid burial (sediment accumulation rates of ca. 2 cm/yr) to depths >10 m, no production during burial and no muonic production since burial, decay of ^{10}Be since burial (constrained by IRSL ages), and a mean surface production rate constrained by middle Pleistocene catchment hypsometry (mean elevation of 420 m). We do not correct for topographic shielding following from Di Biase (2018), who shows that even in steep topography with slopes up to 80° production rates are not significantly different than gentle topography with no shielding. Furthermore, the short Pagliara drainage is not tilted enough to warrant a production rate correction for oblique cosmic rays at depth (Di Biase, 2018).

We isolated and purified quartz at the National Science Foundation/University of Vermont Community Cosmogenic Facility using the approach of Kohl and Nishiizumi (1992), comprising a series of both physical and chemical processes. We then verified quartz purity by Inductively Coupled Plasma—Optical Emission Spectrometry. The samples yielded 13.9 g (sample FJP9) and 21.9 g (sample FJP10) of pure quartz.

We isolated pure Be from the quartz at the National Science Foundation/University of Vermont Community Cosmogenic Facility using the methods described in Corbett et al. (2016). Samples were prepared in a single batch (including eight samples for analysis, two blanks and two quality control standards) during March 2017. We added ca. 250 µg of ^{9}Be to each sample using a beryl-based Be-carrier made in-house with a concentration of 299 µg mL^{-1}.

Accelerator Mass Spectrometry analysis took place at Lawrence Livermore National Laboratory. Sample analyses were normalized to primary standard 07KNSTD3110 with an assumed ratio of 2850×10^{-15} (Nishiizumi et al., 2007). We corrected the sample ratios for backgrounds using the average of the two blanks in the batch ($7.2 \pm 5.4 \times 10^{-16}$) and propagated uncertainties in quadrature.

3.4 | Inversion of fluvial topography

We use the stream power rule of fluvial incision into bedrock to invert the fluvial topography of the Pagliara catchment and reconstruct a history of base level fall (Gallen, 2018; Goren et al., 2014; Pavano & Gallen, 2021). The inversion modelling reconstructs changes in base level fall (e.g. uplift) over the same time frame represented by deposition in the Pagliara fan-delta. In this way, the modelling provides a basis for inferring how changes in tectonic forcing (exogenic) are recorded in the fan-delta stratigraphy.

Our approach follows from Goren et al. (2014) assuming a uniform block uplift, but accounts for cases of variable or uniform rock erodibility. We define the fluvial topography of the Pagliara catchment using a LiDAR data-derived 2-m resolution DEM and set a total of twelve experiments with 1000 Monte Carlo iterations, considering different upslope channel threshold areas ranging from 0.125 to 1 km^2 (Montgomery & Foufoula-Georgiou, 1993; Wobus et al., 2006), variable concavity index, response time discretization and erosion rates. The inversion is carried out in MATLAB using codes developed for a related study in northern Sicily and Apennines and available on GitHub (Pavano & Gallen, 2021; https://github.com/sfgallen/Block_Uplift_Linear_Inversion_Models) and Zenodo (Fisher et al., 2022; https://zenodo.org/record/6503006#.Y8FY0tLMI9F), respectively. These codes work in concert with the MATLAB-based TopoToolbox (Schwanghart & Scherler, 2014, 2017) and TAK (Forte & Whipple, 2019) software packages.

13652117, 2024, 1, Downloaded from https://onlinelibrary.wiley.com/doi/10.1111/bre.12845 by Uni Federico II Di Napoli, Wiley Online Library on [17/01/2024]. See the Terms and Conditions (https://onlinelibrary.wiley.com/terms-and-conditions) on Wiley Online Library for rules of use; OA articles are governed by the applicable Creative Commons License

The theoretical basis and application for our linear inversion approach is well described in several recent publications, some of which are applied to Italian landscapes, and we refer the interested reader to these as well as the supplementary information (SI 2) for a deeper understanding of the approach (Gallen, 2018; Goren et al., 2014; Pavano & Gallen, 2021; Pazzaglia & Fisher, 2022). Critical to the interpretation of the reconstructed base level fall histories is our decision to interpret catchment erosion as a measure of mean rock uplift, a purely detachment-limited channel erosion process consistent with the exponent on slope in the stream power law equal to one ($n=1$; Hancock et al., 1998; Howard, 1994), leading to a simple, linear relationship between the observables of channel steepness (k_{sn}) and erosion (E) and rock erodibility (K).

$$k_{sn} = (E/K)^{1/n} \quad (1)$$

Importantly under this assumption, all changes in the rate of base level fall are preserved because knickpoints propagate at a velocity proportional only to upstream drainage area. Stream steepness is directly measured from the DEM and we calculate it using different concavity values, ranging between 0.4 and 0.5, including the standard reference channel concavity of 0.45 (Snyder et al., 2000). We measure *ks* directly from *chi*-transformed long profiles and E from new and published TCN (Terrestrial Cosmogenic Nuclides) data (Cyr et al., 2010). Following from the assumption that E closely mirrors uplift rate (U) in our system, we can also use the marine terrace geomorphic markers to provide an alternative E estimation. In summary, our model considers E values ranging from 1 to 2 mm/yr resulting in K values that vary by a factor of 2. In reality, channels in the Pagliara catchment experience both detachment-limited (plucking) and sediment abrasion processes where the assumption of $n=1$ may not hold. Non-linearities among stream steepness and channel erosion increasingly emerge as sediment in the channel triggers threshold-depended erosion process and rates of base level fall approach 1 mm/yr (Kirby & Whipple, 2012; Lague, 2013). Both of these criteria characterize the Pagliara catchment, yet the linear assumption among stream steepness and erosion rate has been shown to successfully predict knickpoint location and age throughout the Peloritani Mountains (Pavano et al., 2016), so we proceed with using Equation (1), cognizant of the fact that the model predictions are first-order estimates.

In summary, the inversion model discovers deviations from the steady-state predicted elevation of the Pagliara's channels based on the assumptions above and the actual elevations which are impacted by transient knickpoints and rock-type changes. Considering and removing the impact of rock-type influences in K allows the model to interpret the difference in the steady-state profile from actual channel elevation as unsteadiness in base level fall, expressed as changes in channel steepness and knickpoints propagating upstream from the point of base level fall that is set by the coastline by the Taormina fault.

Model output is the history of base level fall, which in reality is a combination of high-frequency glacio-eustasy and glacial isostatic adjustment (GIA) as well as low-frequency unsteadiness in the rate of rock uplift or subsidence. Model base level in phase with the known glacio-eustatic change would be interpreted to mean that the response time of the Pagliara source-to-sink system is short, and capable of recording both short-term eustatic and longer-term tectonic processes contributing to the integrated base level fall history (Pavano et al., 2016). In contrast, model base level out of phase with known glacio-eustatic change would be interpreted to mean that the response time of the Pagliara source-to-sink system is sufficiently long such that the eustatic processes are shredded by shorter-term geomorphic processes, and the base level fall history is dominated only by tectonic forcing.

4 | RESULTS: SEDIMENTOLOGY AND STRATIGRAPHY OF THE DELTA SYSTEMS

In this section, we first present the main facies and sub-facies, as well as their assemblages, recognized in the field during sedimentological and stratigraphic surveys, which we carried out to analyse the MGS clastic deposits in the area of Pagliara River (Figures 3a–d and 4a,b and Table 1). Then, we pass to describe the general structure and delta systems arrangement of the Pagliara delta complex.

4.1 | Facies description

4.1.1 | Prodelta deep-water chaotic facies (PD)

The Rocchenere delta system base exposes a coarse-grained, poorly sorted and poorly stratified, locally chaotic, thick- to massively bedded sandy gravel prodelta facies (PD) (Figures 3a and 4; see also the stratigraphic column of Figure 3b). In detail, the PD facies is composed of clast-supported pebbles and cobbles with a granule and coarse sand matrix, lacking distinct sedimentary structures. Three distinct sub-facies are recognized (Table 1). The dominant of these are chaotic clastic deposits (PD_a) (Figure 3a), texturally characterized by fine-to-coarse sands, with embedded pebbles and rare cobbles that are locally more abundant. The

13652117, 2024, 1, Downloaded from https://onlinelibrary.wiley.com/doi/10.1111/bre.12845 by Uni Federico II Di Napoli, Wiley Online Library on [17/01/2024]. See the Terms and Conditions (https://onlinelibrary.wiley.com/terms-and-conditions) on Wiley Online Library for rules of use; OA articles are governed by the applicable Creative Commons License

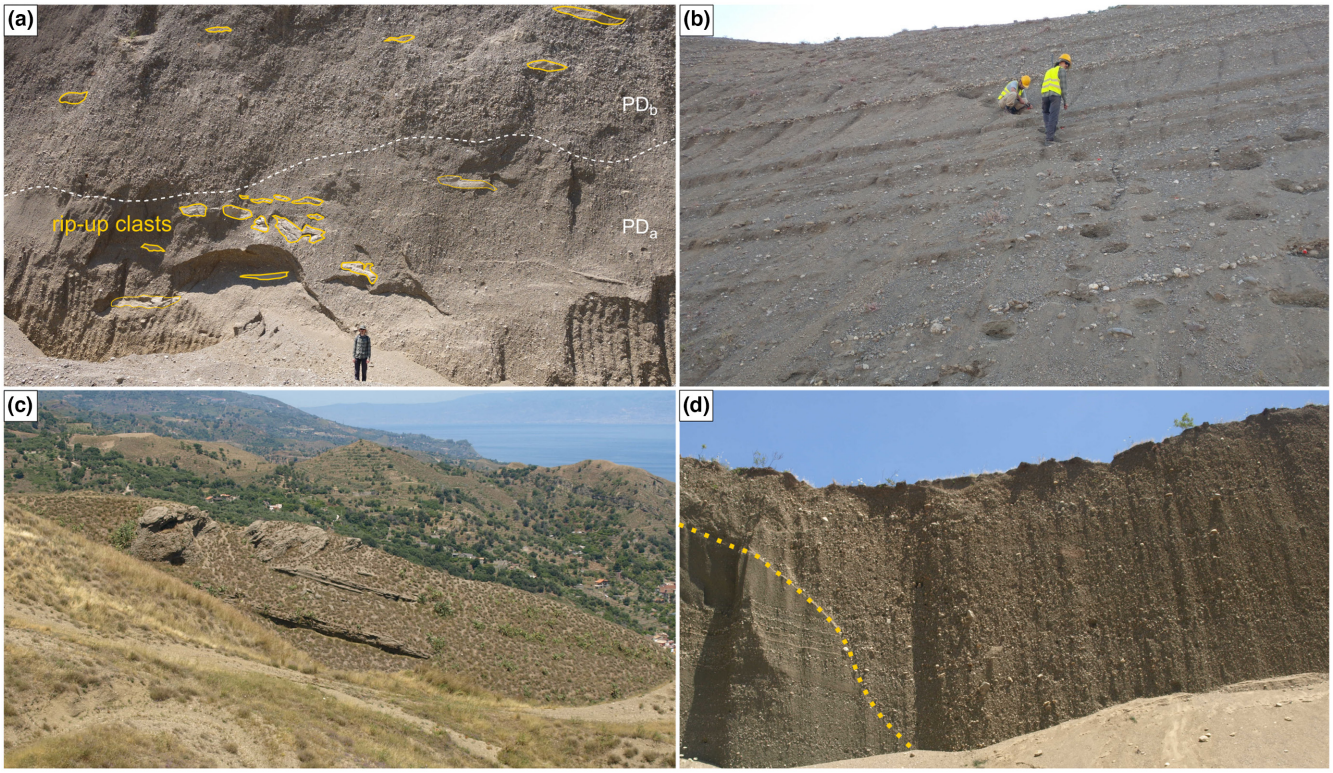

FIGURE 3 (a) quarry vertical wall showing the thick prodelta, deep-water, massive and chaotic deposits, locally course-grained and containing m-scale rip-up clasts (sub-facies PD_a and PD_b). (b) Distributary mouth bar (DMB) layered clastic facies of delta foresets composed of turbidite and gravity flow deposits. (c) Panoramic view of delta plain topsets beds of distributary mouth channels deposits. (d) Upper delta plain, coastal plain and fluvial depositional facies, lying against a steep-walled buttress unconformity (dotted yellow line). The unannotated version of the field photos is reported in SI 3.

minor facies (PD_b) are lenses of coarse-grained clastic sediments, represented by pebbly and cobbly conglomerates (with rare boulders) in a granule and sand matrix. The PD_b facies is weakly stratified (Figure 3a), resulting from the rhythmic transitional, poorly marked passage between dm-thick conglomeratic layers and medium sands with pebbles horizons. At several levels, both the PD_b the PD_a facies contain up to several-metre-long wedges of dm-thick mud horizons, deformed and chaotically mixed in the deposit. These muddy rip-up bodies (Figure 3a) are consistent with deep-water basin deposits scraped from the seafloor or delta plain mudstone transported by mass-wasting events tumbling down the fan-delta front. The PD_a and PD_b deposits grade upward and laterally to a third, less represented sub-facies (PD_c) (Figure 4a–c), made of stratified, thinly bedded sand, fine sand and silty sand.

4.1.2 | Delta front and distributary mouth bar facies

Stratigraphically above the PD facies are distinct, steeply bedded, basin-dipping foreset-bottomsets composed of stacked distributary mouth bar deposits (DMB) (Table 1). The DMB bedsets are gravelly sand that rhythmically fine upwards from pebble and cobble conglomerates in a fine and silty sand matrix to fine granule and sand with common, flat, cm-sized clasts. These foresets prograde over the underlying PD facies with a downlapping stratal geometry. The marine depositional nature of these DMB deposits is affirmed by the presence of *Pecten* sp. shells, (Figure 2b) preserved along the base of the foresets (Figure 3b) where they transition into bottom sets.

The DMB facies contain dm-scale trough cross-stratification with chute-pool backsets (Alexander et al., 2001; Cartigny et al., 2014; Lang & Winsemann, 2013; Postma et al., 2020) (Figure 2e). These cross-beds can be generated in different ways including during DMB progradation in shallow water under alternating oscillatory and unidirectional currents (Dumas & Arnott, 2006), alternating supercritical-to-subcritical flows (Tinterri, 2011), or density flow flood bars (Mutti et al., 2000) that may be triggered by tempestites as the result of storms (Aigner, 1985; Ettensohn et al., 2012; Harms et al., 1975). We note that these bedforms are most consistent with foresets in the

13652117, 2024, 1, Downloaded from https://onlinelibrary.wiley.com/doi/10.1111/bre.12845 by Uni Federico II Di Napoli, Wiley Online Library on [17/01/2024]. See the Terms and Conditions (https://onlinelibrary.wiley.com/terms-and-conditions) on Wiley Online Library for rules of use; OA articles are governed by the applicable Creative Commons License

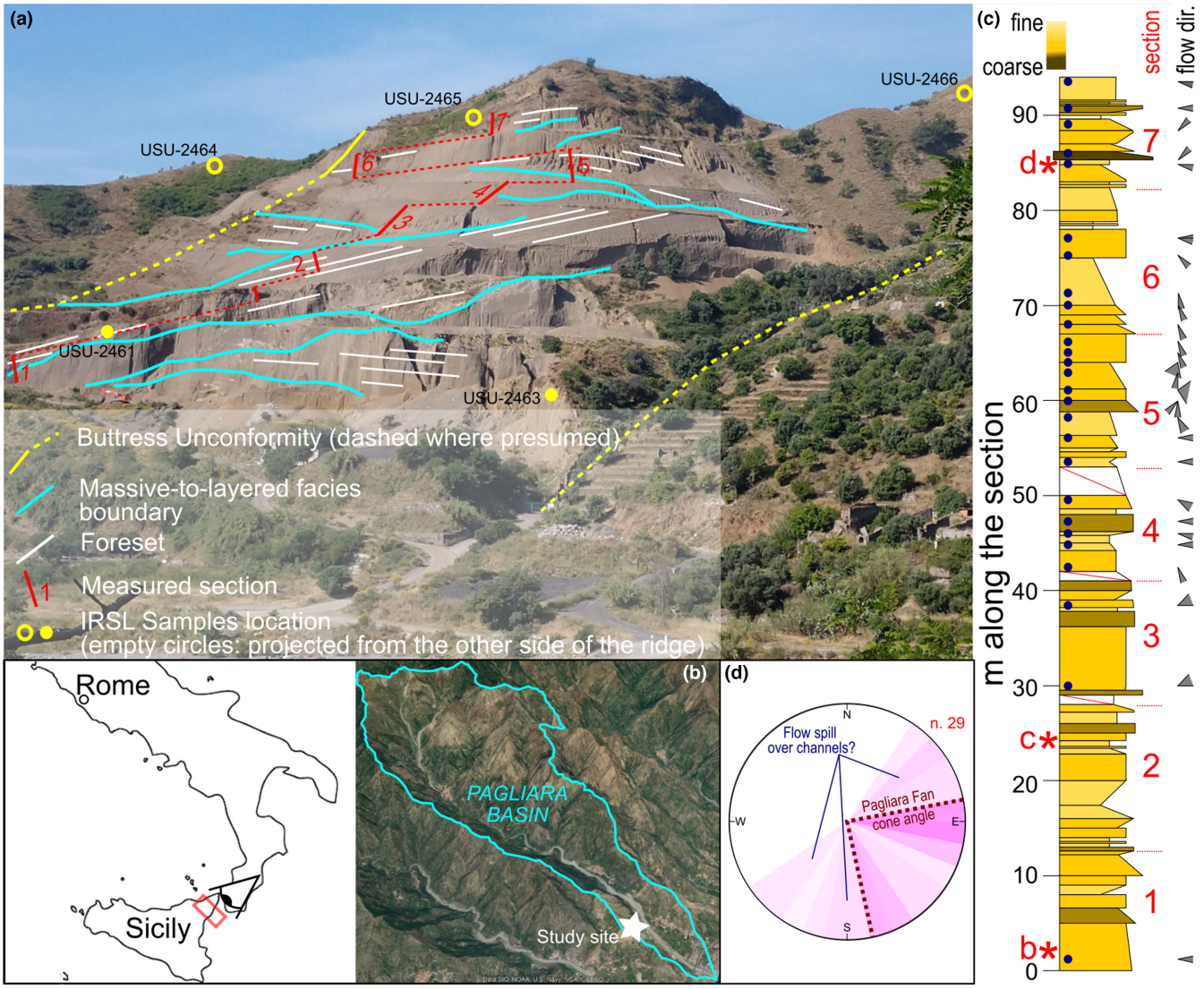

FIGURE 4 (a) Photo showing a panoramic view of the sedimentary architecture of the Rocchenere delta system fan-delta deposits of the Messina Gravel and Sands Formation located at the outlet of the tight source-to-sink system of the Pagliara basin (b). Sequence and facies boundaries, as well as foresets layering, measured sections and IRSL samples location are also reported. The sampled stratigraphy shows alternation of massive and stratified sedimentary facies, stacked in coarsening-up metre-scale bed sets with opposing dips. Numbers refer to the sampled sections of the sequence. The unannotated version of the photo is reported in SI 3; (c) the reconstructed and simplified stratigraphic section is also shown by a colour's palette according with the deposits' grain size. The numbers in red refer to the corresponding portion of the measured section, whereas the red asterisks with letters refers to the location along the section of the corresponding facies shown in the pictures of Figure 3b–d above. The dark blue dots represent the gauging stations for sedimentological measurements, whereas the differently open grey triangle, side of the stratigraphic column, indicates the measured paleo-flow direction. Note that the tringles are open towards the paleo-flow direction and their openness is related to the total angle range provided by multiple measures at the same gauging location. (d) Rose diagram showing the paleo-flow direction (shaded area) measurements ($n = 29$) carried out at different locations along the stratigraphic sequence (c). More intense colour corresponds to more represented azimuths. Overlapped is the Pagliara fan cone angle (dotted dark red lines).

delta front even though they are similar in some respects to tidal-generated bedforms present in the sandwaves of the MGS exposed near Messina. The Rocchenere delta system DMB facies lack the typical sigmoidal structures of the tidally dominated deposits (Boersma & Terwindt, 1981; Mutti et al., 1984, 1985) and the overall orientation is transverse, rather than sub-parallel to the shore (Longhitano, 2018).

4.1.3 | Delta plain facies

The DMB facies are overlain, and locally scoured and inset by lower delta plain topset beds composed primarily of distributary mouth channels (DMC; Figures 2a and 3c). These facies have good lateral continuity and are characterized by fining-upward, dm-thick bedsets, composed of pebbles and cobbles organized in clast-supported but

13652117, 2024, 1, Downloaded from https://onlinelibrary.wiley.com/doi/10.1111/bre.12845 by Uni Federico II Di Napoli, Wiley Online Library on [17/01/2024]. See the Terms and Conditions (https://onlinelibrary.wiley.com/terms-and-conditions) on Wiley Online Library for rules of use; OA articles are governed by the applicable Creative Commons License

TABLE 1 Description of the major textural and structural features of the facies and sub-facies recognized in the MGS deposits at the Pagliara delta complex.

Facies associations	Facies	Sub-facies	Facies description
Coastal plain and fluvial facies (CPF)	Coastal plain facies		Poorly stratified and organized deposits, interleaved with medium-to-thick beds of fine gravel and very coarse sand. Locally, along buttress unconformity, these deposits contain dm- to m-size boulders
	Fluvial facies		Fluvial deposits show coarser and rounded, discoid and equant pebbles. The structure is generally defined by pebbles and granules supported by abundant fine-to-coarse sandy matrix; some horizons show clast-supported, open framework structure. Structures of clasts imbrication, according to the paleo-currents, are common
Delta plain facies (DMC)			Fining-upward, dm-thick bedsets, composed of pebbles and cobbles organized in clast-supported but closed framework conglomerate with a very coarse sand matrix. Upward, these deposits pass to cm-thick beds of coarse to very coarse sandy matrix-supported flat pebble conglomerate
Delta front and distributary mouth bar facies (DMB)			Steeply bedded, basin-dipping foreset-bottomsets with a downlapping stratal geometry, composed of gravelly sand rhythmically fining upwards from pebble/cobble conglomerates, in a fine and silty sand matrix, to fine granule and sand with flat, cm-sized clasts. Pecten sp. Shells are found
Prodelta deep-water chaotic facies (PD)		PD_c	Stratified clastic deposits, composed of thinly bedded sand, fine sand and silty sand
		PD_b	Weakly stratified clastic deposits with lenses of coarse-grain sediments, represented by pebbles and cobbles conglomerates (with rare boulders) in a granule and sand matrix. Chaotically mixed in the deposits are muddy rip-up bodies
		PD_a	Chaotic clastic deposits composed of fine-to-coarse sands, with embedded pebbles and rare cobbles (locally abundant). Chaotically mixed in the deposits are muddy rip-up bodies

closed framework conglomerate with a very coarse sand matrix. These conglomerates rapidly grade upward to cm-thick beds of coarse to very coarse sand matrix-supported flat pebble conglomerate (Table 1). Locally, m-thick layers of these deposits sub-horizontally truncate eastward-dipping, dm-layered DMB bedsets and are in turn inset by channels filled with coarse-grained sediments, cobble-pebbles in size.

4.1.4 | Coastal plain and fluvial facies (CPF)

The fan-delta facies are inset by upper delta plain, coastal plain and fluvial depositional facies (Table 1), locally along steep-walled buttress unconformities (CPF; Figures 3c, 4a, and 5a). This facies is dominated by stacked and cross-cutting fluvial channels. Unlike the delta facies, the CPF are more poorly stratified and organized instead of beds of matrix-supported pebbles and cobbles interleaved with medium-to-thick beds of fine gravel and very coarse sand. Locally, especially in contact with the buttress unconformity, the CPF deposits contain large, dm- to m-size boulders. In summary, the CPF exhibit an onlapping stratal geometry with the fan-delta facies.

CPF facies is clearly represented by fluvial deposits showing coarser and rounded, discoid and equant pebbles. The structure of these conglomerates shows layers of pebbles and granules supported by abundant fine-to-coarse sandy matrix, but some horizons show clast-supported, open framework structure. Sedimentological structures are commonly represented by clasts imbrication according to the paleo-currents (see inset rose diagram and stratigraphic column in Figure 4d), mainly pointing towards east and southeast. Inset fluvial clastic wedges outcrop at different elevations through the depositional body, filling paleo-channel morphologies shaped on DMB facies deposits as clear unconformities (Figure 3c,d).

4.2 | Description of the architecture of the Pagliara delta complex: The Pagliara and the Rocchenere delta systems

The field-based sedimentological and stratigraphic analysis of the MGS deposits in the area of the Pagliara Basin reveals that they consist of several nested and partially stacked Gilbert-type fan-deltas. These fan-deltas have an

13652117, 2024, 1, Downloaded from https://onlinelibrary.wiley.com/doi/10.1111/bre.12845 by Uni Federico II Di Napoli, Wiley Online Library on [17/01/2024]. See the Terms and Conditions (https://onlinelibrary.wiley.com/terms-and-conditions) on Wiley Online Library for rules of use; OA articles are governed by the applicable Creative Commons License

apparent large-scale cyclical architecture both as landforms and in stacking of facies that generally conforms to a sequence stratigraphic model (Figures 4 and 5a,b). Delta facies suite ranges from fluvial-coastal plain, delta front and prodelta environments, to facies transitional to an open basin environment. Fossiliferous horizons served as key layers in the field to recognize the transgressive maximum flooding surfaces (MFS in Figure 5a). These key horizons, together with lower, bounding buttress unconformities, allowed the recognition of sequences, the vertical and lateral geometrical relationships of those sequences, as well as the depositional environment in the context of variable boundary conditions. Field observations (Figure 4) and remote-sensed images reveal that the Pagliara delta complex is composed of two different nested fan-delta systems (Figure 5a). The upper fan-delta system, hereafter called the Pagliara delta system, is inset by a lower fan-delta, hereafter called Rocchenere delta system, along a bedrock buttress unconformity carved into the metamorphic bedrock (Figure 5). The overall body of the lower Rocchenere delta system shows a higher gradient in the seaward general geometry resulting from the nestling of at least two, probably three, delta fans (Figure 5a), with the topsets located at variable elevations (230–330 m a.s.l.).

The Pagliara delta system is likely composed of several main sedimentary bodies ca. 150–170 m thick, with poorly exposed contacts, that prograde and telescope seaward atop a gently sloping or stepping bedrock strath, as observed in the field (Figures 4 and 5). By contrast, the well-exposed Rocchenere delta system consists of at least three nested, telescoping fan-delta bodies separated by large (ca. 40–60 m) topographic drops that collectively define a seaward-dipping basal strath that is inferred to be steeper than that of the Pagliara delta system (Figure 5b). The basal wave-cut platform hosting the entire Rocchenere delta system progradational sequence does not crop out, because it is extensively buried beneath the recent alluvial deposits of the Pagliara River, except locally at the bedrock buttress unconformity that separates the Rocchenere delta system from the Pagliara delta system.

The exposed Rocchenere delta system deposits (stratigraphic column in Figure 4), following an upsection shallowing of the depositional environment, can be generally organized into upper delta plain fluvial and coastal plain facies (FCP), lower delta plain-distributary mouth channel (DMC) facies, delta front distributary mouth bar (DMB) delta front facies and deep-water prodelta (PD) facies (Figures 2a,c,e and 3a–d). Along the Rocchenere delta system analysed section, field-based sedimentologic analyses reveal variations and sometimes almost abrupt switching, in paleo-flow directions measured for different bedsets belonging to stacked delta lobes (Figure 4). Specifically, a lower, dominant east-directed flow switches, during the deposition of section 5 and most of section 6 (Figure 4), to SSE-to-SW directions and locally to NE directions upsection during the deposition of section 7 (Figure 4). However, the most common detected paleo-flow-directions fall within the general SE-directed Pagliara fan-delta complex cone (Figure 4).

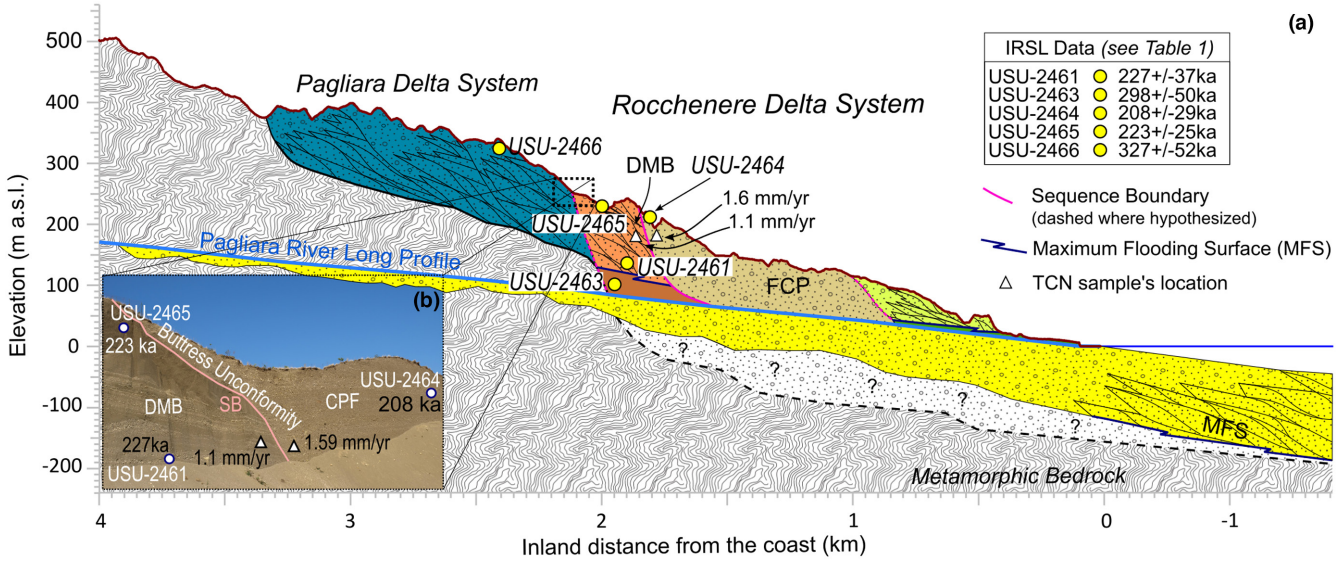

FIGURE 5 (a) Stratigraphic model of the Pagliara fan-delta showing the relationships between the different allostratigraphic units. IRSL ages (circles) and TCN paleo-erosion rates (triangles) are keyed into their sampling sites. The resulting IRSL ages and relative errors are also reported. (b) Photo of the quarry highwall annotated with specific features depicted in (a), showing the buttress unconformity that separates the DMB facies of samples USU-2461 and USU-2465 from the fluvial/coastal plain deposits sampled at site USU-2464 (see (a) for reference).

13652117, 2024, 1, Downloaded from https://onlinelibrary.wiley.com/doi/10.1111/bre.12845 by Uni Federico II Di Napoli, Wiley Online Library on [17/01/2024]. See the Terms and Conditions (https://onlinelibrary.wiley.com/terms-and-conditions) on Wiley Online Library for rules of use; OA articles are governed by the applicable Creative Commons License

5 | RESULTS: GEOCHRONOLOGY AGE MODEL AND PALEO-EROSION RATES

5.1 | Luminescence age model

Samples dated using IRSL (Table 2) provide stratigraphically coherent ages, indicating that the entire Rocchenere delta system depositional succession analysed in this study ranges over ca. 119 kyr, from 326.9 ± 37.3 ka (sample USU-2466) to 208.0 ± 29.1 ka (sample USU-2464) (Figure 5a,b and Table 2) and from coastal plain/fluvial and distributary mouth channel facies to distributary mouth bar facies up to prodelta/delta front units. The main Rocchenere delta system depositional body was deposited in ca. 75 kyr, between 297.6 ± 49.8 (USU-2463) and 223.1 ± 24.9 ka (USU-2465), at a mean sediment accumulation rate (SAR) of ca. 0.15 cm/yr. Luminescence D_E values are close to the characteristic dose of saturation (D_0, Table 1), which can lead to age underestimation. However, as discussed below, the luminescence ages are in stratigraphic order, conform to sedimentologic and stratigraphic constraints observed in the field and align with projections to eustatic sea level controlled accommodation space that control delta preservation, suggesting that any age underestimation within the data are within reported errors.

In general, the depositional sequence is carved and nested by younger parasequences, opening towards the sea at lower elevations (Figures 4 and 5a). In particular, basal prodelta chaotic facies with an IRSL age of 297.6 ± 49.8 ka (sample USU-2463; Table 2) are sharply, but conformably overlain by younger marine DMB facies, with an age ranging between 226.6 ± 37.4 and 223.1 ± 24.9 ka (samples USU-2461 and USU-2465, respectively; Table 2) (Figure 5a,b). This allostratigraphic package is inset by younger coastal plain and fluvial facies deposits dated to 208.0 ± 29.1 ka (sample USU-2464) (Figure 5a,b and Table 2), with an associated 1σ error partially overlapping the other fluvial and DMB ages. The ca. 3.5 kyr time gap between the IRSL dates of samples USU-2461 and sample USU-2465, collected within the same DMB facies, and their elevation gap of ca. 87 m, provide an estimate of the fastest SAR of ca. 2.5 cm/yr.

5.2 | Cosmogenic ^{10}Be paleo-erosion rate data

Cosmogenic ^{10}Be concentrations of shielded sediment sampled at the 223.1 ± 24.9 ka delta distributary mouth bar facies and the 208.0 ± 29.1 ka fluvial-coastal plain facies across the buttress unconformity (Figure 5a,b) are used in concert with the IRSL depositional age of these deposits to calculate paleo-erosion rates. The measured ^{10}Be concentrations (N_t) (Table 3) are increased to their decay-corrected burial values (N_o) using the ^{10}Be decay constant of 4.3 e−09 yr^{-1}. The DMB and CPF facies provided values of 1.1 ± 0.17 and 1.59 ± 0.75 mm/yr, external uncertainties, respectively (Table 4). These values are still comparable with the modern Pagliara basin-wide erosion rate of ca. 1.0 ± 0.1 mm/yr (Cyr et al., 2010), as well as the uplift and erosion rates estimation published in previous studies (ca. 1.6 mm/yr; Pavano et al., 2016).

6 | RESULTS: BASE LEVEL HISTORY FROM AN INVERSION OF FLUVIAL TOPOGRAPHY MODEL

The long profile inversion modelling (Figures 6 and 7a–c) predicts a base level fall history for the Pagliara catchment. That base level fall integrates eustasy, rock uplift (or subsidence) of the catchment, as well as deposition, erosion and propagation of the Rocchenere-Pagliara delta

TABLE 2 Infrared-stimulated luminescence (IRSL) age information.

Sample num.	USU num.	Num. of aliquots[a]	Dose rate (Gy/kyr)	Fading rate g_{2days} %/decade (n)	Equivalent dose[b] ± 2σ (Gy)	Mean $2D_0$ (Gy)[c]	IRSL age[d] ± 1σ (ka)
OSL 6.1	USU-2464	12 (24)	4.05 ± 0.21	2.48 ± 0.32 (12)	841.6 ± 39.9	849	208.0 ± 29.1
OSL 7.1	USU-2465	13 (17)	3.34 ± 0.18	2.99 ± 0.30 (6)	745.9 ± 78.3	915	223.1 ± 24.9
OSL 1.1	USU-2461	18 (25)	3.52 ± 0.18	2.58 ± 0.25 (8)	795.5 ± 50.1	869	226.6 ± 37.4
OSL 5.1	USU-2463	12 (16)	3.53 ± 0.14	3.14 ± 0.39 (11)	1059.9 ± 111.1	892	297.6 ± 49.8
OSL 8.1	USU-2466	11 (18)	3.64 ± 0.25	3.57 ± 0.30 (6)	1189.4 ± 112.4	1224	326.9 ± 37.3

[a]Age analysis using the single-aliquot regenerative-dose procedure of Wallinga et al. (2000) on 2 mm small-aliquots of potassium feldspar sand at 50°C IRSL. Number of aliquots used in age calculation and number of aliquots analysed in parentheses.

[b]Equivalent dose (D_E) corrected for fading (loss of signal) following the methods of Lamothe et al. (2003) and reported as the weighted mean of aliquot values.

[c]IRSL age calculated by dividing the fading-corrected D_E by the environmental dose rate.

[d]Mean characteristic dose of saturation ($2D_0$) are provided as a reference to how close the De values are to the maximum value that can be accurately obtained from a sample due to saturation. The weighted mean De values fall below the $2D_0$ value for each sample except OSL 5.1, which is within error of $2D_0$.

13652117, 2024, 1, Downloaded from https://onlinelibrary.wiley.com/doi/10.1111/bre.12845 by Uni Federico II Di Napoli, Wiley Online Library on [17/01/2024]. See the Terms and Conditions (https://onlinelibrary.wiley.com/terms-and-conditions) on Wiley Online Library for rules of use; OA articles are governed by the applicable Creative Commons License

TABLE 3 Cosmogenic ^{10}Be paleo-erosion rate sample preparation data, calculation of ^{10}Be concentration and uncertainties.

Sample name	Quartz mass (g)	Mass of ^{9}Be added (μg)[a]	AMS cathode number	Uncorrected ^{10}Be/^{9}Be ratio[b]	Uncorrected ^{10}Be/^{9}Be ratio uncertainty[b]	Background-corrected ^{10}Be/^{9}Be ratio	Background-corrected ^{10}Be/^{9}Be ratio uncertainty	^{10}Be concentration (atoms g^{-1})	^{10}Be concentration uncertainty (atoms g^{-1})	^{10}Be uncertainty %
FJP9	13.9459	245.7	BE42308	2.890E−15	8.484E−16	2.165E−15	1.009E−15	2.55E+03	1.19E+03	46.57
FJP10	21.8928	245.6	BE42309	5.651E−15	3.899E−16	4.926E−15	6.703E−16	3.69E+03	5.02E+02	13.61

[a]^{9}Be was added through a beryl carrier made at University of Vermont with a concentration of 298.7 μg mL^{-1}.

[b]Isotopic analysis was conducted at Lawrence Livermore National Laboratory; ratios were normalized against standard 07KNSTD3110 with an assumed ratio of 2850×10^{-15} (Nishiizumi et al., 2007).

TABLE 4 Cosmogenic ^{10}Be paleo-erosion rate modelling.

Sample name	Lat (°)	Long (°)	Elev (m a.s.l.)	^{10}Be decay constant uncertainty	^{10}Be half-life uncertainty (years)	Age of dated TCN sample	$N(t)$	N_o	N_o uncertainty	Erosion rate (m/my)	Erosion rate uncertainty (m/my)
FJP9	37.972	−78.029	85	4.30E−09	11,929.14	226,000	2.55E+03	2854.37	1329.41	1.59	0.75
FJP10	37.972	−78.029	85			208,000	3.69E+03	4097.87	557.60	1.1	0.17

Note: The used ^{10}Be decay constant and ^{10}Be half-life are 5.0E−07 and 1,386,555 (years), respectively.

13652117, 2024, 1, Downloaded from https://onlinelibrary.wiley.com/doi/10.1111/bre.12845 by Uni Federico II Di Napoli, Wiley Online Library on [17/01/2024]. See the Terms and Conditions (https://onlinelibrary.wiley.com/terms-and-conditions) on Wiley Online Library for rules of use; OA articles are governed by the applicable Creative Commons License

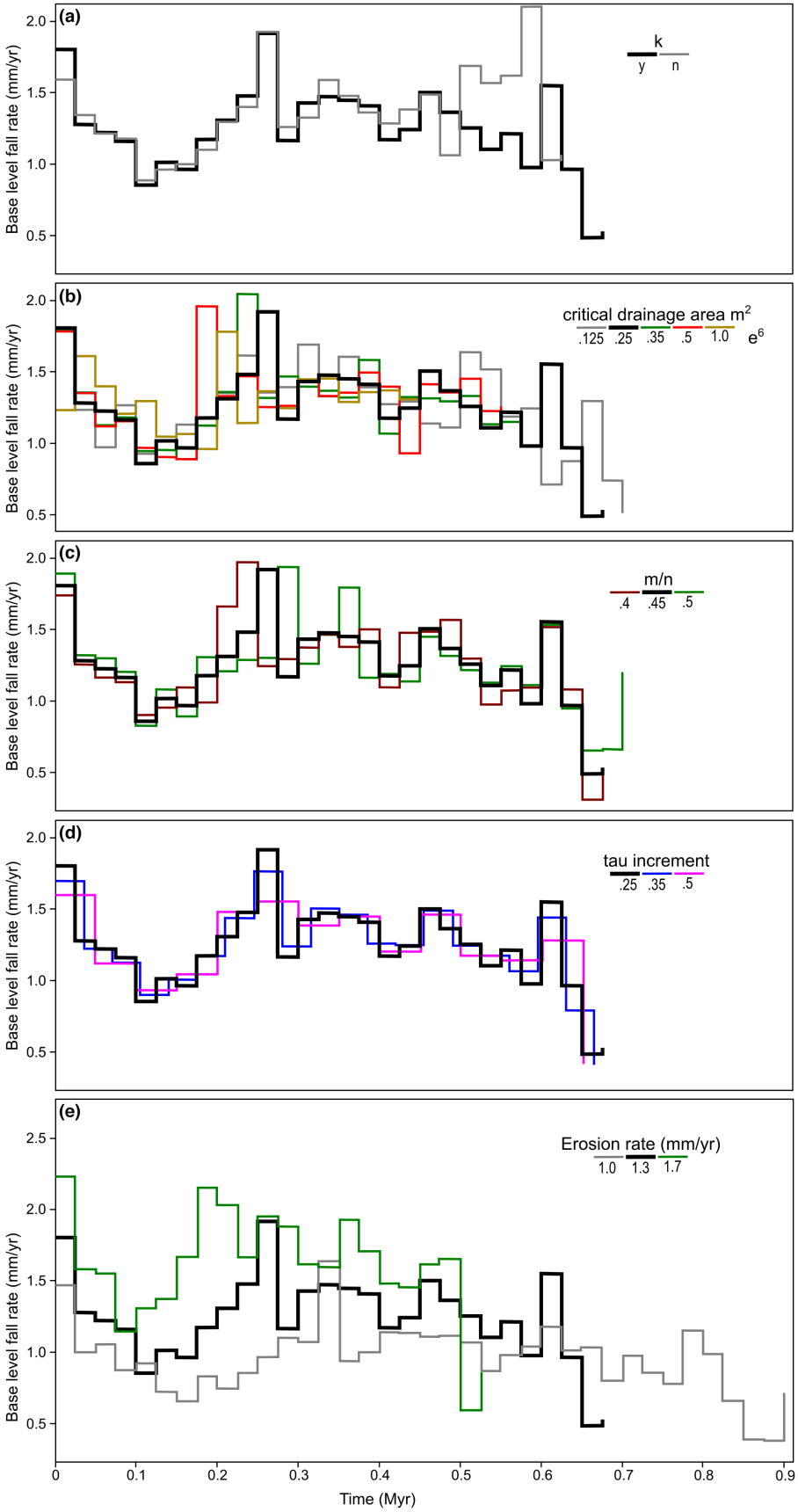

FIGURE 6 Results and comparisons of the different setting applied for the long profile inversions of the Pagliara drainage system. (a) Base level fall rate-time plots obtained by accounting (*y*) or not (*n*) lithological variations; (b) using different values in critical drainage area, (c) concavity index (*m*/*n*), (d) tau increments and (e) by accounting for different values of erosion rates.

13652117, 2024, 1, Downloaded from https://onlinelibrary.wiley.com/doi/10.1111/bre.12845 by Uni Federico II Di Napoli, Wiley Online Library on [17/01/2024]. See the Terms and Conditions (https://onlinelibrary.wiley.com/terms-and-conditions) on Wiley Online Library for rules of use; OA articles are governed by the applicable Creative Commons License

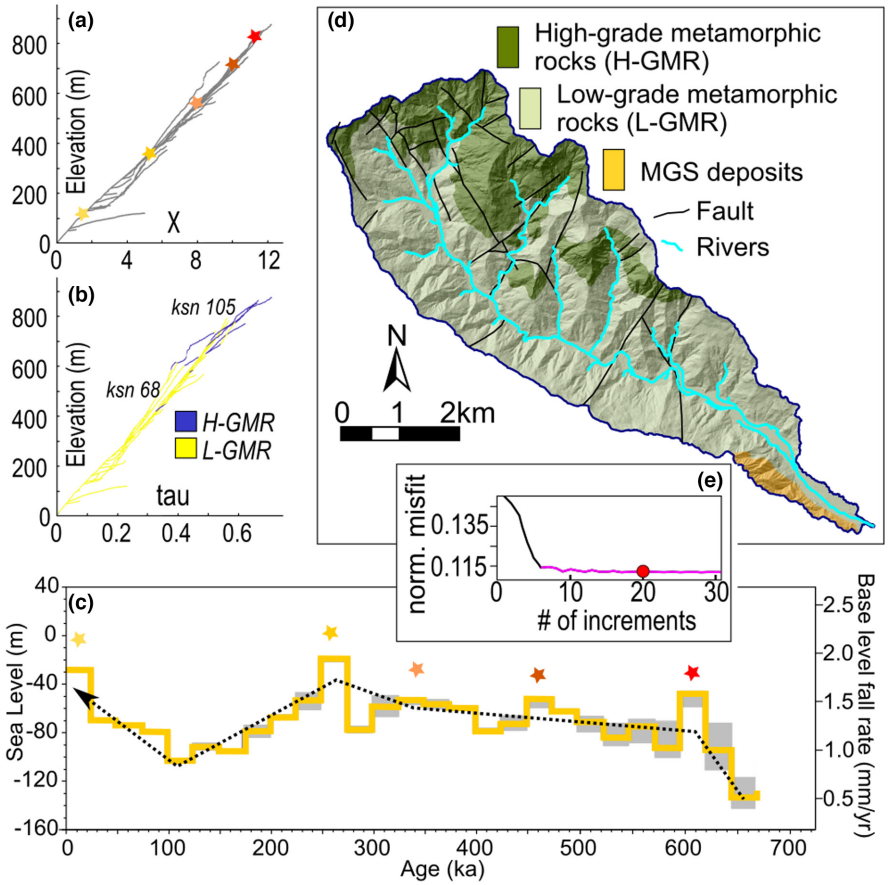

FIGURE 7 (a) χ-elevation plot (Chi plot) of the Pagliara basin's watershed. The grey lines represent the observed streams profiles. The coloured stars indicate the location of change in k_{sn}, corresponding to the slope change of the modelled long profile in the χ-elevation space (knickpoint). These knickpoints are paired with the corresponding peaks in the base level fall rate-time plots shown in (c); (b) tau-elevation plot coloured basing on the different rock types, high-grade (H-GMR) and low-grade (L-GMR) metamorphic rocks; (c) step plot showing the Pagliara watershed's long profile inversion results for the reconstruction of the base level fall history encoded in the geomorphic record, obtained using the values in bold in Table 5. The grey shaded portion of the plot shows the misfits of the inversion derived from a total of 1000 iterations run by a Monte Carlo approach; (d) geological map of the Pagliara watershed, also showing the analysed drainage network; (e) results of the sensitivity test run to find a reliable number of χ increments to discretize the inverted river long profiles. The plot shows a wide zone of low misfit when the long profiles are inverted using >10–15 increments with the minimum misfit provided by discretizing the profile in 20 increments. Each increment corresponds to a χ-interval of ca. 300.

systems. We assemble several models that explore the parameter space of the input variables as a means of creating an ensemble result with uncertainties (Table 5).

In Figure 6a–d we show the results of a model sensitivity analysis carried out by comparing the various base level fall reconstructions. We show our choice of reasonable parameters in generating the U-tau data that, most suitably describes the base level fall history of the Pagliara region within geologic constraints and the lowest model misfits. In Figure 6e we compare the base level fall histories reconstructed for the selected values of variables (in bold in Table 5), but considering different long-term erosion rates.

We run 1000 iterations for each combination of the considered variables in Table 5. We find that the results of the inversion model for the Pagliara watershed changes very little due to K (Figure 6a), since actually the inverted fluvial topography is mostly homogeneous, underlain by the same low-grade metamorphic rock type (Figure 7b,d). The model results are less sensitive to variation in concavity index and to critical drainage area, which impact on the total response time (Figure 6b,c). In summary, the data obtained by using $\theta = 0.45$, variable K, a critical drainage area of 0.25 km^2 and a tau interval of 25 kyr, provides the best detailed reconstruction of the base level fall history with the lowest misfits (Figure 7e), and those will be the model parameters we will use and discuss hereafter in the paper.

Lastly, we explore the impact of different values of long-term erosion rates (E mm/yr) on the reconstruction of the base level fall history of the Pagliara watershed (Figure 6e). We test three values of E, 1.0, 1.3 and 1.6 mm/

13652117, 2024, 1, Downloaded from https://onlinelibrary.wiley.com/doi/10.1111/bre.12845 by Uni Federico II Di Napoli, Wiley Online Library on [17/01/2024]. See the Terms and Conditions (https://onlinelibrary.wiley.com/terms-and-conditions) on Wiley Online Library for rules of use; OA articles are governed by the applicable Creative Commons License

Critical drainage area[a] (km^2)	θ[b]	Tau interval[c] (kyrs)	Variable K	E (mm/yr)
0.125	0.40	**25**	***y***	1.0 ± 0.1
0.25	**0.45**	35	*n*	**1.3 ± 0.1**
0.35	0.50	50		1.6 ± 0.1
0.50				
1.00				

TABLE 5 Input variables used to perform long profile inversion analysis.

Note: In bold are the selected values for each variable that we use in the model results discussed below and showed in Figure 7c.

[a]Basin drainage area needed for fluvial initiation.

[b]Profile concavity.

[c]Model step in time.

yr. The first and the last values crudely match our two paleo-erosion values (Table 4). In particular, the 1.1 mm/yr value is compatible with paleo-erosion rate from previous works (Cyr et al., 2010), whereas the 1.6 mm/yr value matches the uplift rate proposed by previous studies for the late Pleistocene period based on marine terraces and river long profile analyses (Catalano et al., 2008; Catalano & De Guidi, 2003; Pavano et al., 2016). The 1.3 mm/yr value that we test crudely approaches the average between the two values inferred by our cosmogenic ^{10}Be paleo-erosion rate data. The results predictably indicate that the overall response time of the model scales linearly with the chosen E (a function of $n = 1$). Additionally, by using an E value of 1.3 mm/yr, the resulting response time for Pagliara matches the middle-late Pleistocene onset of the uplift and emersion history of northeastern Sicily predicted by previous studies (Catalano & Di Stefano, 1997; Pavano et al., 2018).

The model parameterized with the selected values (in bold in Table 5) indicates that between 650 and 250 ka the mouth of the Pagliara watershed experienced multiple base level rise and fall at rates ranging from ca. 2.0 to 0.7 mm/yr. This trend, with an average of ca. 1.30 mm/yr and gently increasing towards the present (Figure 7d), also has a quasi-periodic behaviour spanning ca. 100–150 kyr (Figure 7d). However, at ca. 200–250 ka, the model indicates a pulse in base level fall of ca. 1.9 mm/yr, followed by a rapid rise and a slowing of rates to ca. 0.9–1.0 mm/yr at 125–150 ka, before increasing again up to the present to a rate of ca. 1.8 mm/yr. An important final consideration in our modelling is that the alluviated downstream sector of the Pagliara's river bed (extending up to ca. 2 km upstream from the coastline; Figure 4) could have been affected by lateral shifts of base level up to ca. 2 km during glacial–interglacial periods. The Pagliara delta is ca. 2 km inland indicating that the shoreline has extended seaward that distance over the past 200 ka. Lateral shifts in base level technically violate the basic assumptions of our modelling approach, so we test the impact of the point of base level fall in our long profile inversion analysis and show the results in the supplementary information (SI 4). Specifically, we chose a point of base level fall ca. 2.5 km upstream from the present coastline that eliminates the lower, presently alluvial segment that would have corresponded more or less to the coastline at the time of Pagliara delta deposition. We find that the results of this experiment are not different from models that choose the modern coastline as the point of base level fall, except for small changes in the overall response time of the model (SI 4). Because the lower Pagliara channel carries the largest discharge, and our model assumes a response time inverse to discharge and drainage area, lateral shifts in base level of several kilometres at the mouth of the river, and their attendant small (m-scale) vertical elevation changes for a prograding coastline have little effect on model results. Similarly, large base level falls, such as those driven by glacio-eustatic drawdown, effectively are pinned at similar locations within 2 km of the modern coastline given the steep, seaward-facing escarpment of the Taormina fault footwall. Therefore, the model that we present and interpret below chooses the current coastline as a simplified, but representative fixed point of base level fall.

7 | DISCUSSION

7.1 | Base level history from a delta depositional model

The Pagliara delta complex, composed of the upper Pagliara delta system and the lower, inset Rocchenere delta system (Figure 8a) supports a depositional model dominated by variable creation and loss of accommodation space at the foot of the Peloritani Mountains. In both cases, the Pagliara delta system and the Rocchenere delta system indicate periods when accommodation space was created by a combination of eustatic rise and tectonic

13652117, 2024, 1, Downloaded from https://onlinelibrary.wiley.com/doi/10.1111/bre.12845 by Uni Federico II Di Napoli, Wiley Online Library on [17/01/2024]. See the Terms and Conditions (https://onlinelibrary.wiley.com/terms-and-conditions) on Wiley Online Library for rules of use; OA articles are governed by the applicable Creative Commons License

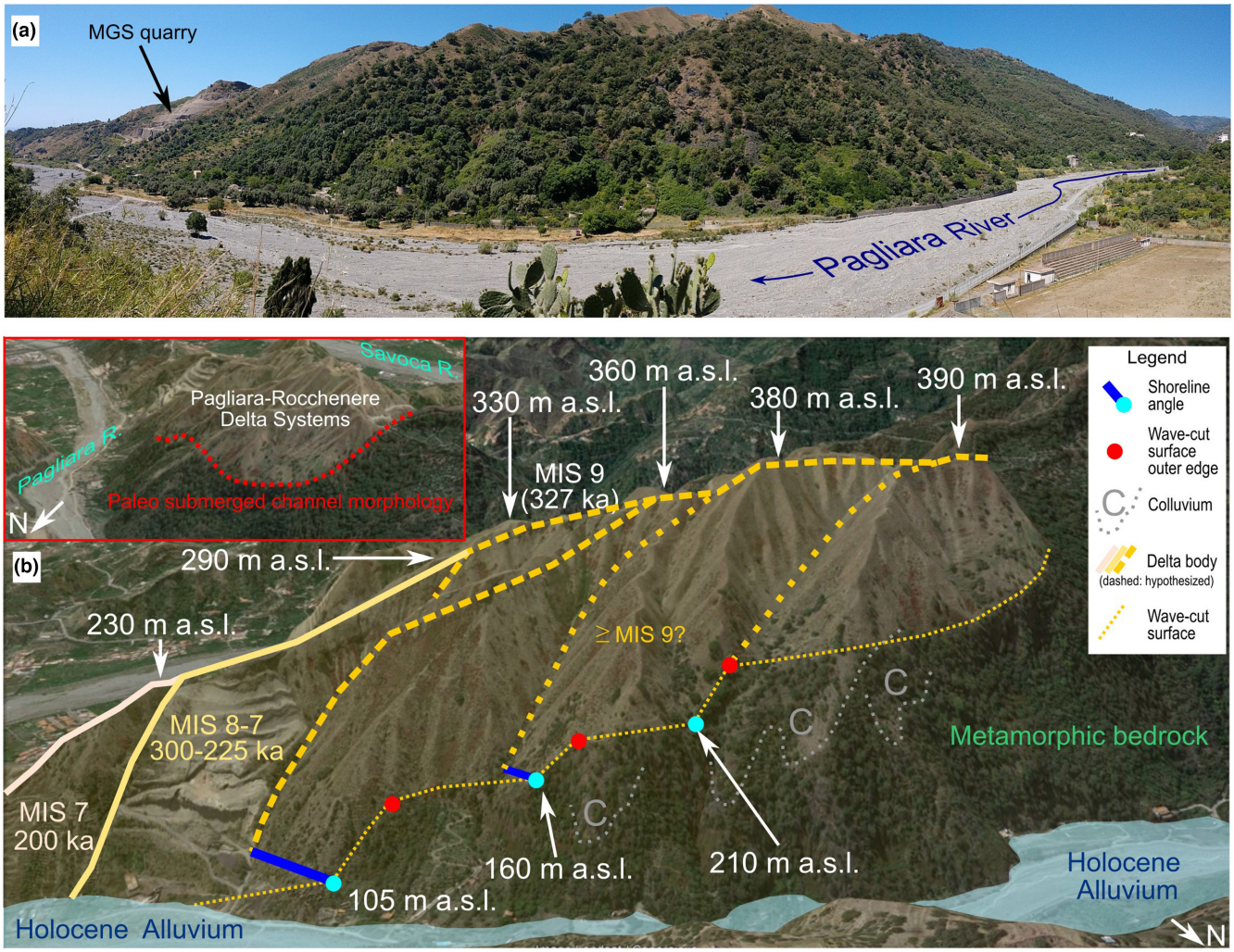

FIGURE 8 (a) panoramic overview (southward) of the southern flank of the lower Pagliara River valley, capped by the clastic deposits of Pagliara delta system and Rocchenere delta system. The location of the MGS quarry is also reported; (b) view (Google Earth) of the Pagliara delta complex, with outlined the main geomorphic and stratigraphic elements of the depositional model, as inspired by the luminescence-based age model. The inset shows the Pagliara MGS deposits (associable with ≥ MIS 10) viewed from rear (upstream), highlighting their relationships with the paleo-morphology, shaped in the metamorphic bedrock.

subsidence. The inset nature of the Rocchenere delta system to the Pagliara delta system and the exposure of both now several hundred metres above sea level indicate the current loss of that accommodation space and a tectonic inversion of a former hanging wall basin. The modern coastal plain and assumed Holocene high stand delta is 5 km seaward of the Rocchenere delta system and being constructed on what appears to be a bathymetric cliff we interpret as the footwall escarpment of the Taormina fault. It is notable that the only thick MGS deposits occur at the mouth of the Pagliara catchment and in the region around Messina (Figure 1d), which we interpret to reflect the termini of a former range-bounding normal fault segment ramp prior to the assembly of the modern Taormina fault.

The Pagliara delta system, likely composed of multiple but poorly exposed individual delta bodies, was emplaced as forward-telescoping deposits on a gently seaward-dipping bedrock surface corresponding to a former hanging wall ramp basin of the Taormina fault. The relationship of the uppermost clastic body of the Pagliara delta system with the bedrock shows a channel-fill-like geometry (inset in Figure 8b), suggesting the deposition in an upper delta plain-distributary channel environment. The age of the Pagliara delta system is only known to be greater than or equal to MIS 8 (Figure 8b). According to our depositional model, the Pagliara delta system deposits could be envisioned as partially reworked during younger sea level rises.

The general architecture and geomorphic position of the Pagliara delta system indicates deposition during a time of relative base level stability (Figures 6 and 7), or slow base level fall, likely slower than present rates. Accommodation space during this time was likely created

13652117, 2024, 1, Downloaded from https://onlinelibrary.wiley.com/doi/10.1111/bre.12845 by Uni Federico II Di Napoli, Wiley Online Library on [17/01/2024]. See the Terms and Conditions (https://onlinelibrary.wiley.com/terms-and-conditions) on Wiley Online Library for rules of use; OA articles are governed by the applicable Creative Commons License

by transient rises in base level generated by quasi-periodic tectonic subsidence or eustatic rise (Figure 9a), or both.

In contrast, the much better exposed and dated Rocchenere delta system could have only been deposited during a brief period of accommodation space creation as sea level rose rapidly during MIS 7. This relative base level rise and creation of accommodation space is superimposed on a longer-term period of base level rise driven

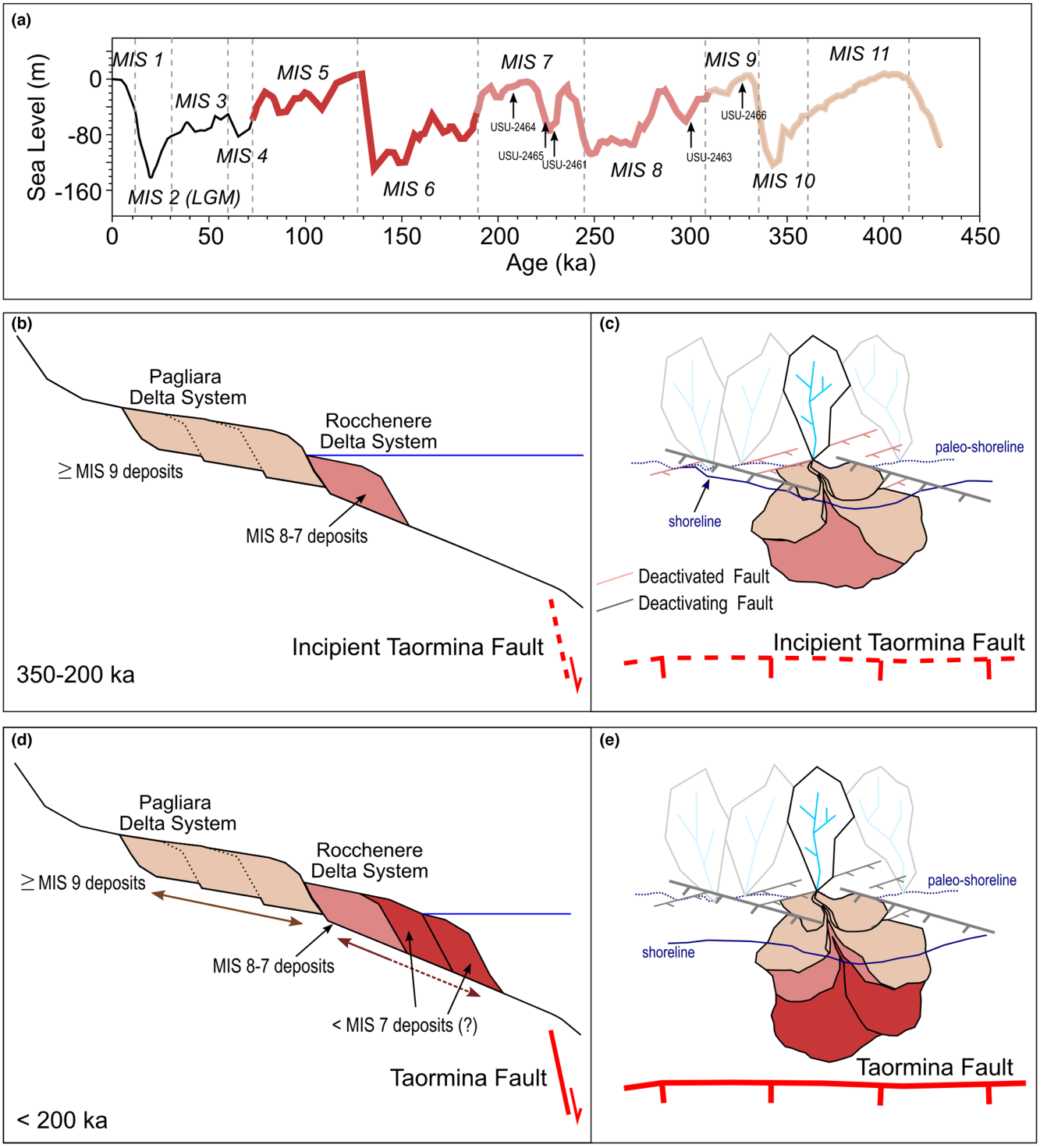

FIGURE 9 (a) Reference eustatic curve (Waelbroeck et al., 2002) reporting each depositional event of the Pagliara depositional complex (pictured in b–e). The IRSL samples position are also reported (black arrows) (see table in Figure 5a for the samples' codes reference). Cartoon showing a simplified overview, both in cross-section (b, d) and plan view (c, e), of the sedimentary and tectonic evolution in building the Pagliara delta complex during the middle-late Pleistocene (<350 ka) along the Ionian coast of the Peloritani Mountains. The double arrowed brown lines highlight the different distribution slope of the two delta systems.

13652117, 2024, 1, Downloaded from https://onlinelibrary.wiley.com/doi/10.1111/bre.12845 by Uni Federico II Di Napoli, Wiley Online Library on [17/01/2024]. See the Terms and Conditions (https://onlinelibrary.wiley.com/terms-and-conditions) on Wiley Online Library for rules of use; OA articles are governed by the applicable Creative Commons License

by tectonic subsidence of the former hanging wall ramp basin. Rocchenere delta system deposition represents delta progradation into a deep basin whose floor, unlike the floor of the Pagliara delta system basin(s) is mostly not exposed. Our IRSL ages indicated that progradation commenced during MIS 8 as deep-water, chaotic delta front facies that are abruptly transgressed by a marine flooding surface that preserves marine *pectin* sp. fossils, presumably during the rapid rise of sea level during the latter half of MIS 7. The accommodation space created during that rise stacked delta front foreset and lower delta plain deposits more or less vertically as the coastline must have temporarily stabilized as a balance between sediment derived from the source and relative base level. Deposition continued for ca. 5 ka concluding with the progradation of upper delta plain facies prior to MIS 6 at 208 ka.

Subsequently, base level fall ensued during MIS 6, driven primarily by uplift but also by eustatic fall, resulting in incision and partial exposure of the Rocchenere delta system (Figure 8b). Subsequent unsteady exhumation of the Rocchenere delta system was punctuated by the carving of marine terraces into the delta sediments during sea level still-stands during MIS 5 (Catalano & De Guidi, 2003). Rapid base level fall commenced and continued to the present, serving to push the shoreline farther east and uplift the entire Pagliara delta system and Rocchenere delta system deltas since <MIS 7 (Figure 9b–e).

In summary, the geomorphic expression of the deltas, the facies models and the numeric age model all indicate a creation of accommodation space (relative subsidence) equal or prior to MIS 10, followed by rapid loss of accommodation space after MIS 8 punctuated only by a brief period of renewed delta deposition, the Rocchenere delta system, that was clearly driven by the MIS 7 eustatic sea level rise.

7.2 | Integration of base level history from delta deposition and source inversion

The sedimentologic, stratigraphic and geochronologic data in the Pagliara delta system and Rocchenere delta system coupled with the inversion of fluvial topography allow us to present an integrated base level fall history for the Pagliara section of the Peloritani Mountains and explore how tectonics are encoded in the stratigraphy and geomorphology of coupled source-to-sink systems.

With these data, and within the constraining assumptions of the inversion model, we are able (i) to constrain the glacial-to-interglacial timing of deposition and history of base level fall, (ii) to recognize the proximity of the nearshore marine depositional environments, (iii) to distinguish and interpret different fluvio-deltaic facies and their spatial distribution, (iv) to explore and model the role of tectonic in building a stratigraphic and geomorphic records in a source-to-sink system.

7.2.1 | Source-to-sink process coupling

We reconstruct an integrated history of base level fall for the mouth of the Pagliara catchment from down-basin sedimentology and stratigraphy in the sink and an up-basin inversion of fluvial topography in the source (Figure 10).

From the perspective of the river channels in the Pagliara catchment (red line in Figure 10a) the mouth of the Pagliara basin experienced a quasi-periodic base level fall history that is in phase with the global, non-GIA-corrected eustatic record from 650 to 250 ka. We note that over this time period minima in the rate of base level fall correspond to maxima in the sea level curve (averaged for 25kyrs intervals and showed as blue step-line in Figure 10b). The precise phase shift between the base level curve (red line) and the eustatic curve (blue line) is sensitive to the erosion rate that we chose for the inversion model. The solution shown here in Figure 10 serves to illustrate the point that with small adjustments in response time due to variable rock erodibility (K) or deviation from a linear model where the power dependency on slope (n) is not 1, it is easy to see how the base level fall history for this early time period is fully consistent with eustatic changes superimposed on a slow and even steadily uplifting Peloritani footwall.

It is difficult to compare the >250 ka part of the base level fall history directly to the Rocchenere delta system or Pagliara delta system delta because it mostly precedes their deposition. But what limited information we know about the Pagliara delta system is consistent with the idea of a relatively steady tectonic (ca. 1.3 mm/yr) forcing for the >250 ka time frame, probably representing the regional component of uplift (Catalano et al., 2008; Catalano & Di Stefano, 1997; Di Stefano & Caliri, 1996; Pavano et al., 2015, 2018). During this time frame, periods of eustatic highs or, alternatively, periods of tectonic subsidence, allowed for the creation of accommodation space (Figure 10c) and the emplacement of the Pagliara delta system on a relatively gently dipping bedrock floor. We note that impulsive base level fall at the mouth of the Pagliara should be preserved in the knickpoints of the catchment's fluvial topography, and there should be a correlation between geomorphic markers at the coast, like the Pagliara delta system or older marine terraces and those knickpoints. This is precisely the observation noted by Pavano et al. (2016) and it argues that for catchments undergoing rapid base level fall

13652117, 2024, 1, Downloaded from https://onlinelibrary.wiley.com/doi/10.1111/bre.12845 by Uni Federico II Di Napoli, Wiley Online Library on [17/01/2024]. See the Terms and Conditions (https://onlinelibrary.wiley.com/terms-and-conditions) on Wiley Online Library for rules of use; OA articles are governed by the applicable Creative Commons License

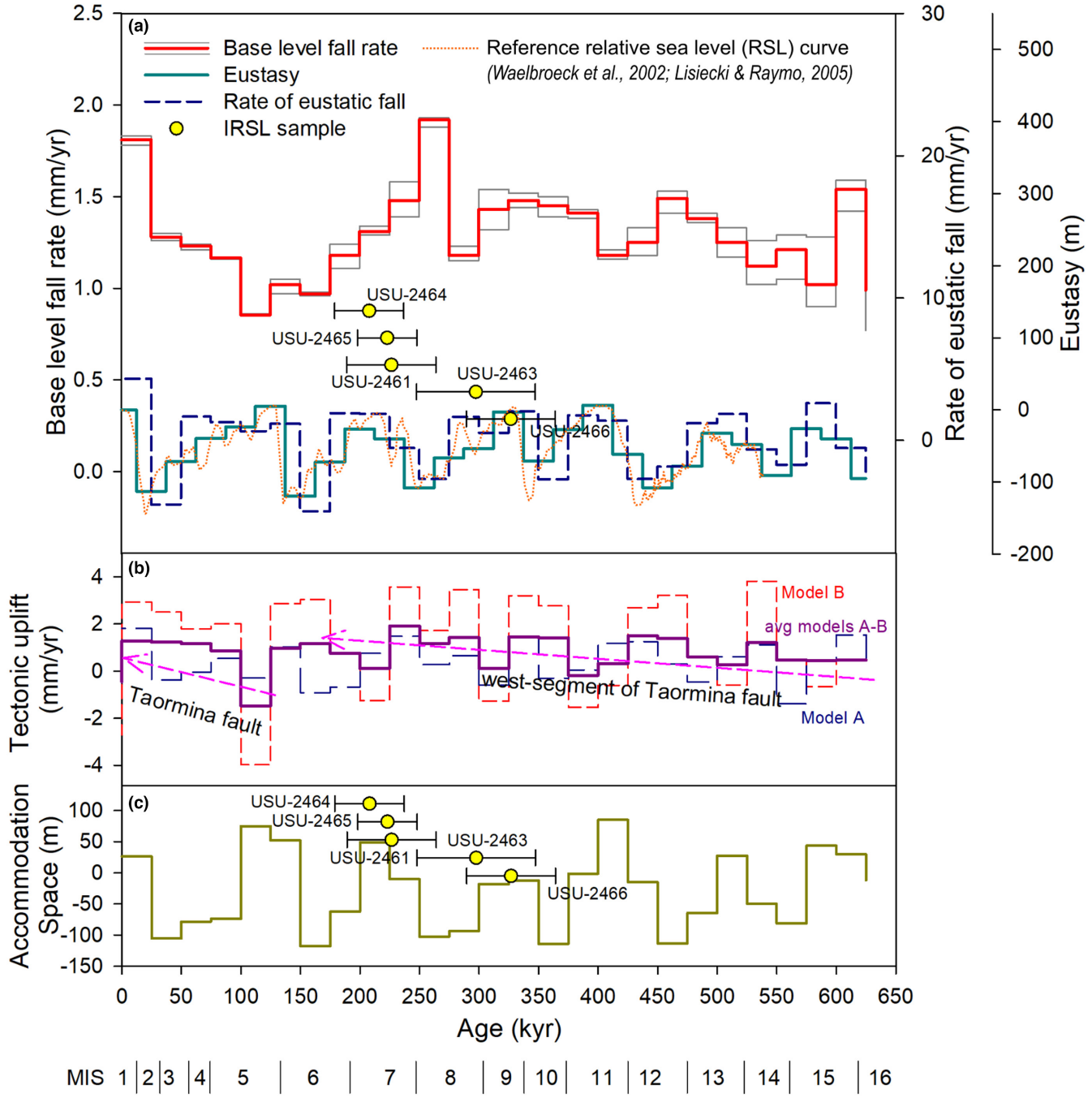

FIGURE 10 (a) Base level fall rate curve (red step top plot, corresponding to the thick black step curve in Figure 6), reconstructed by long profile inversion analyses, plotted against the middle-late Pleistocene eustatic relative sea level (RSL) changes (dark green curve in the lower plot); the RSL changes data are plotted in terms of rate (dashed blue step curve in the lower plot). These data are used to calculate the rate of eustatic fall (dark blue dashed step-line in the lower plot). The reference relative sea level (RSL) curves are from Waelbroeck et al. (2002) and from Lisiecki and Raymo (2005) (orange dotted line). (b) The plot represents the results of the subtractions of eustasy from the base level fall rate history (red line in a) according to two different models, model A (blue dashed-line step plot) and model B (dashed-line red step plot) and the average of the two models (purple step plot). The luminescence data (yellow circles) and their associated errors are also reported; (c) Plot showing the resulting accommodation space (m), calculated as the difference between the tectonically produced uplift and the space created by eustasy.

(uplift) where system's response times are short, it may be possible for high-frequency eustasy to be preserved in the source topography (c.f. Gallen & Fernández-Blanco, 2021; Godard et al., 2013; Snyder et al., 2002), unless the DTM resolution is not suitable to capture the knickpoints' sizes (Pavano & Gallen, 2021).

13652117, 2024, 1, Downloaded from https://onlinelibrary.wiley.com/doi/10.1111/bre.12845 by Uni Federico II Di Napoli, Wiley Online Library on [17/01/2024]. See the Terms and Conditions (https://onlinelibrary.wiley.com/terms-and-conditions) on Wiley Online Library for rules of use; OA articles are governed by the applicable Creative Commons License

In contrast, from the perspective of the river channels in the source, there is an impulse of rapid base level fall at 250 ka at a rate approaching 2 mm/yr, followed by a deceleration to a minimum of ca. 0.9 mm/yr at 100 ka and then an acceleration to ca. 1.7 mm/yr at present (Figure 10a). This broad saddle shape in the source-determined base level fall is not easily matched to maxima and minima of the corresponding sea level curve. For example, the MIS 6 sea level low should correspond to an increase in the rate of base level fall, but it does not. Similarly, the subsequent rapid MIS 5e eustatic rise should be recorded as a slowing in the rate of base level fall, but it barely registers as such.

Here the deposition of the Rocchenere delta system is comparable to the fluvial topography inversion results. The time of rapid Rocchenere delta system deposition coincides with slow rate of base level fall during the entire base level reconstruction. Given the periodic eustatic lows also during this time interval, it is possible that there was tectonic subsidence such that the subsidence partially negated the effects of the eustatic drawdowns. This makes sense for the perspective of the thick delta deposits that must have accumulated in a basin undergoing transient subsidence.

At this point, we proceeded by filtering from the modelled base level fall rate history (Figure 10a) the eustasy component of the relative sea level (RSL) changes. In order to do this, we firstly converted the eustatic oscillation (m) (green step-line in Figure 10a) into a rate (mm/yr) (dashed dark blue step-line in Figure 10a). Depending on the difference in rate between the sea level rise and the tectonic uplift, the obtained residual BLF rate could be still considered a combination of two components, the tectonic uplift rate and the rate of sediments accumulation; this latter is assumed counterbalancing the accommodation space created by subsidence and resulting in an alluvial river profile adjusted to the long-term E-U steadiness (1.3 mm/yr). In this way, we obtained an estimation of the tectonic uplift rate history net of eustasy and sediment accumulation (Model A—dashed blue step-line in Figure 10b). An alternative and more simplified model (Model B—dashed red step-line in Figure 10b) consider the simple removal of the eustasy signal from the modelled base level fall history. This simplified model, although resulting in a tectonic uplift history showing a trend similar to that provided by Model A, argues for higher values in the tectonic component and wider variations in uplift/subsidence cycles (Figure 10b). An intermediate tectonic uplift rate history for the Pagliara system has been finally obtained (solid purple step-line in Figure 10b) by averaging the rates obtained by the two models (model A and B). These averaged results still show the general two branches trend reconstructed by both model A and model B.

For all the three different tectonic uplift rate histories, it is not to exclude the role played in creating space by minor én-echelon-distributed faults (Figure 9c) (west-segment of Taormina fault in Figure 10b), thought as the early surficial expression of the incipient deformation along the Taormina fault, with associated relay ramps-related deformations (e.g. Leeder & Jackson, 1993) (Figure 9c). The increasing accommodation space (Figure 10c), matches the general fining-upward sedimentary texture through the analysed sequence, topped by a coarser-grain sedimentary cap related to the facies suite's retreat (Figures 3c and 4).

Conversely for the time period younger than ca. 125 ka, there is nothing but an acceleration in base level fall despite general eustatic rise (Figure 10a). This can only be explained by rapid tectonic uplift, presumably as the footwall of the (re-)activated Taormina fault (Figures 9e and 10b).

7.2.2 | Expression of tectonic processes in the depositional and geomorphic records

Having demonstrated that the base level fall history for the Pagliara catchment is consistent in records assembled in the source and the sink, we here discuss how specific tectonic forcing is encoded, or not, in the delta deposits. We restrict our discussion on this topic to the Rocchenere delta system because exposures of the Pagliara delta system are not sufficient to draw firm conclusions.

Tectonics and eustasy are the principal factors controlling the denudational processes in the source, the accommodation space in the sink, and the facies distribution and the shape of delta systems (Galloway, 1975) as well as their dynamics (e.g. lobe switching) (Coleman, 1975; Seybold et al., 2007). In our case, particularly for the accommodation space, the tectonic uplift factor works antithetically with the RSL changes, since the Pagliara delta complex is assumed to be entirely hosted in the footwall block of the Taormina fault. The tectonic contribution of the development of the Pagliara delta complex mainly manifests in driving the general architecture and the vertical-lateral relationships of the delta bodies, as well as the spatiotemporal juxtaposition of different sedimentary facies. The tectonic control in forging the fluvial topography results in a long-term growing relief and rapid changes in base level fall during the middle-late Pleistocene (<250 ka) evolutionary stage of Pagliara system, as well as in the higher-gradient architecture of the nested, lower Rocchenere delta system's bodies (Figure 9).

In experimental studies, increased uplift rate corresponds to an initial pulse in grain size coarsening, slowly recovered moving upward in the section (Rohais et al., 2012). Uplift also corresponds to an increase in

13652117, 2024, 1, Downloaded from https://onlinelibrary.wiley.com/doi/10.1111/bre.12845 by Uni Federico II Di Napoli, Wiley Online Library on [17/01/2024]. See the Terms and Conditions (https://onlinelibrary.wiley.com/terms-and-conditions) on Wiley Online Library for rules of use; OA articles are governed by the applicable Creative Commons License

sediment supply and in delta bed thickness, together with a general development of down lap sedimentary geometries. Extending those concepts to our natural experiment, the basal facies of chaotic and massive coarse-grain deposits, interleaved with prodelta and deep-water environment deposits, could correspond to the initial stage of basin filling of the increasing accommodation space (200–250 ka; Figures 9 and 10c).

Following from a Bull-inspired process-response model (Bull, 1991) the hillslopes in the Pagliara catchment would be expected to shed more sediment during glacial–interglacial transitions and that sediment would have been effectively trapped and deposited in the Rocchenere delta system by the eustatically produced accommodation space. Although our TCN data are not dense enough to resolve whether erosion has been unsteady over several glacial cycles (e.g. Ott et al., 2022), given the short ^{10}Be integration time as erosion rates approach 1.3 mm/yr of just a few millennia, catchment-scale hillslope soil production and landslide frequency must be relatively uniform and steady even as climate changes. In any event, the unsteady trapping of sediment at the mouth of the paleo-Pagliara River and resulting rapid shallowing of sediment transport slope favoured autogenic processes, leading the temporarily lateral switching and repeat stacking of prodelta and deep-water depositional environment (PD_c facies).

For example, combined slowing uplift rate and eustasy variations, lead to a positive maximum in accommodation space at ca. 200–250 ka (Figure 10c), available to host coarse-grain debris deposits (e.g. MIS 7 coastal plain deposits). The aggradation of coarser sediments is consistent with channel backfilling and backwater avulsion processes, leading distributary channels radial spilling over into small size delta lobes and the partitioning of water and sediment (Coleman, 1975; Feng et al., 2019; Ganti et al., 2014, 2016; Seybold et al., 2007; Van Dijk et al., 2009) (rose diagram and stratigraphic column in Figure 4d). These processes allow the Pagliara delta system to grow by expanding and roaming laterally (Figure 4).

Many previous studies highlighted the occurrence of autogenic behaviour during allogenic processes, or independently of them, and their leading role in delta-fan evolution (Clarke et al., 2008; De Haas et al., 2016; Foreman & Straub, 2017; Kim et al., 2006; Kim & Jerolmack, 2008; Kim & Paola, 2007; Nicholas & Quine, 2007; Schumm et al., 1987; Van Dijk et al., 2009; Whipple et al., 1998). Despite these insights, the scale of stratigraphic observations and the resolution of the analysed geomorphic records in the present study allow us to address the role played by tectonics in concert with climate in leading to variation in accommodation space and the general fluvial-deltaic depositional facies distribution and delta complex architecture. We do not know and can only estimate the boundary conditions (e.g. water and sediment input, type of sediment transport, feeder channel width; Van Dijk et al., 2009) of the Pagliara delta complex at the time of the MGS deposition. Thus, it is difficult to argue and discriminate about the contribution of autogenic vs. allogenic processes in building the Pagliara delta stratigraphy and to associate forms and spatial facies distribution either to autocyclical fan-delta evolution or to climate and/or tectonic perturbation.

Nevertheless, local field observations of m-thick multiple erosion/incision-and-filling depositional cycles (bar and fluvial channel deposits) on top of DMB deposits (e.g. Figure 3c) could represent the evidence of autogenic scouring and backfilling processes as postulated by analogue modelling (e.g. Van Dijk et al., 2009) or just the seaward facies progradation. Similarly, the paleo-flow directions (see stratigraphic section in Figure 4), aligned along orientations out from the fan-delta cone angle of the Pagliara delta complex could be sedimentological evidence of autogenic depositional processes. These changes in paleo-flow direction could represent autogenic cycles-related flow spill-over channelization, due to flow exceeding the confining channel walls during backfilling process (Van Dijk et al., 2009). Alternatively, the detected eccentric paleo-flows could correspond to lateral channel shifting processes due to the formation of bars near larger feeder channel (Clarke et al., 2008; Van Dijk et al., 2009) during the Pagliara delta growth, as also reported in analogue and numerical models (Ashworth et al., 2004, 2007; Bryant et al., 1995; Clarke et al., 2008; Schumm et al., 1987; Seybold et al., 2007; Van Dijk et al., 2009; Whipple et al., 1998).

However, in the Pagliara delta case, the upper delta plain environment could be envisioned as the site of scour initiation (Feng et al., 2019; Kim & Jerolmack, 2008; Van Dijk et al., 2009) and channels development, allowing the sediments transfer to deeper delta environments. This scours initiation belt can be envisioned continuously prograding due to tectonically forced regression, determining the delta plain incision and the channelization of pulses in debris flows and avalanches, which bypass to the delta front environment.

8 | CONCLUSIONS

We applied a multidisciplinary approach to explore the Pagliara fluvio-deltaic stratigraphic record built through a tight, fault-controlled source-to-sink system in the eastern side of the Peloritani Mts. in NE-Sicily (Italy). This work aims at the definition of a geochronologically constrained and numerically predicted late Quaternary

13652117, 2024, 1, Downloaded from https://onlinelibrary.wiley.com/doi/10.1111/bre.12845 by Uni Federico II Di Napoli, Wiley Online Library on [17/01/2024]. See the Terms and Conditions (https://onlinelibrary.wiley.com/terms-and-conditions) on Wiley Online Library for rules of use; OA articles are governed by the applicable Creative Commons License

morphotectonic model. The study particularly was designed to produce solid age model, and stratigraphic and geomorphic constrains to explore the depositional evolution and facies distribution of a natural fan-delta systems framed in the late Quaternary tectonic deformation setting. In the study area, we found that the delta bodies, outcropping up to ca. 300 m a.s.l., are organized in two main nested delta systems, Pagliara and Rocchenere Delta System, lying at the footwall of the Taormina normal fault (Catalano et al., 2008). We geochronologically (IRSL) associate the deposition of the Pagliara delta complex to a complete interglacial–glacial–interglacial cycle (ca. 330-to-200 ka, MIS 9-to-7) period. We explore this stratigraphic record in association with erosion rates data, which roughly match the modern basin-integrated values (Cyr et al., 2010), and with the long-term, ca. 650 ka-long, base level fall history reconstructed for the Pagliara watershed by linear inversions of river profile.

At the scale of observation and analysis, our data argue for an allogenic forcing-driven delta evolution. The reconstructed delta depositional evolution and spatiotemporal facies distribution, and the geomorphic evolutionary model as well, are consistent with eustasy-driven erosional events overlapped to a longer-term (250–650 ka), slightly increasing rock uplift tectonic signal (ca. 1.3 mm/yr). Especially during the last 250 kyr, corresponding with the deposition time of most of the MGS, our data claim for the prevailing role of tectonic, in concert with eustasy, in creating accommodation space, in leading the general stratigraphic architecture of the Pagliara delta complex, and in dampening the eustasy signal by modulating the upstream propagation of fluvial erosional responses. This period of tectonic disturbance can be easily associated with the onset of the (re)activation of the Taormina Fault, parallel to the eastern coast of Peloritani Mts.

Although dominant leading long-term tectonic and/or climate factors in modulating accommodation space in the sink, and erosion processes in the source, it is not possible to falsify the, even partial, autocyclic behaviour in the Pagliara fan-delta evolution, as evidenced in the field by variations in paleo-flow directions and by m-thick channel backfilling deposits. Further investigations focused on the environmental changes periodicities encoded into the Pagliara delta system's stratigraphy will be crucial to unravel the effective conspiration between allogenic and autogenic processes in the fan-delta dynamics and growing.

ACKNOWLEDGEMENTS

The authors would like to thank Editor-in-Chief Professor Atle Rotevatn, and Andrew J. Cyr and an anonymous reviewer for their helpful and constructive comments that improved the earlier version of the manuscript. This research was supported by the NSF-EAR-Tectonics program, in the frame of the project TESPRESSO (*Tectonic Encoding, Shredding and Propagation of Environmental Signals as Surface Observables*), award #1904262 (P.I. Frank J. Pazzaglia). Sample preparation was supported in part by NSF-EAR-1735676 (P.I. Paul Bierman) at University of Vermont/NSF Community Cosmogenic Facility. The authors want to thank Nicole Gasparini, Laurent Roberge and Natalie Tanski for helping in data collection, and Giorgia Boscarino, Sig. R. Cacopardo and Agriturismo Amendolara for logistical support.

CONFLICT OF INTEREST STATEMENT

The author declares that there is no conflict of interest.

DATA AVAILABILITY STATEMENT

The data that supports the findings of this study are available in the supplementary material of this article.

ORCID

P. Bierman https://orcid.org/0000-0001-9627-4601

REFERENCES

Aigner, T. (1985). Storm depositional systems, dynamic stratigraphy in modern and ancient shallow-marine sequences. In *Lecture notes in earth sciences* (Vol. *3*). Springer-Verlag.

Aitken, M. J. (1998). *An introduction to optical dating: The dating of quaternary sediments by the use of photon-stimulated luminescence* (p. 267). Oxford University Press.

Aitken, M. J., & Xie, J. (1990). Moisture correction for annual gamma dose. *Ancient TL*, *8*(2), 6–9.

Alexander, J., Bridge, J. S., Cheel, R. J., & Leclair, S. F. (2001). Bedforms and associated sedimentary structures formed under supercritical water flow over aggradading beds. *Sedimentology*, *48*, 133–152.

Allen, P. A. (2008). Time scales of tectonic landscapes and their sediment routing systems. In K. Gallagher, S. I. Jones, & R. J. Wainwright (Eds.), *Landscape evolution: Denudation, climate and tectonics over different time and space scales* (Vol. *296*, pp. 7–28). Geological Society, London, Special Publications. https://doi.org/10.1144/SP296.2

Allen, P. A., & Allen, J. R. (2013). *Basin analysis: Principles and application to petroleum play assessment* (p. 632). John Wiley & Sons.

Allen, P. A., & Densmore, A. L. (2000). Sediment flux from an uplifting fault block. *Basin Research*, *12*, 367–380.

Amodio Morelli, L., Bonardi, G., Colonna, V., Dietrich, D., Giunta, G., Ippolito, F., Liguori, V., Lorenzoni, S., Paglionico, A., Perrone, V., Piccarreta, G., Russo, M., Zanettini, L. E., & Zappetta, A. (1976). L'arco calabro-peloritano nell'orogene appenninico-maghrebide. *Memorie della Societa Geologica Italiana*, *17*, 1–60.

Amoruso, A., Crescentini, L., & Scarpa, R. (2002). Source parameters of the 1908 Messina Straits, Italy, earthquakefrom geodetic and seismic data. *Journal of Geophysical Research*, *107*(B4), 2080. https://doi.org/10.1029/2001JB000434

13652117, 2024, 1, Downloaded from https://onlinelibrary.wiley.com/doi/10.1111/bre.12845 by Uni Federico II Di Napoli, Wiley Online Library on [17/01/2024]. See the Terms and Conditions (https://onlinelibrary.wiley.com/terms-and-conditions) on Wiley Online Library for rules of use; OA articles are governed by the applicable Creative Commons License

Antonioli, F., Kershaw, S., Renda, P., Rust, D., Belluomini, G., Cerasoli, M., Radtke, U., & Silenzi, S. (2006). Elevation of the last interglacial highstand in Sicily (Italy): A benchmark of coastal tectonics. *Quaternary International*, *145–146*, 3–18.

Argnani, A., Brancolini, G., Bonazzi, C., Rovere, M., Accaino, F., Zgur, F., & Lodolo, E. (2009). The results of the Taormina 2006 seismic survey: Possible implications for active tectonics in the Messina Straits. *Tectonophysics*, *476*, 159–169.

Armitage, J. J., Duller, R. A., Whittaker, A. C., & Allen, P. A. (2011). Transformation of tectonic and climatic signals from source to sedimentary archive. *Nature Geoscience*, *4*(4), 231–235. https://doi.org/10.1038/NGEO1087

Ashworth, P. J., Best, J. L., & Jones, M. (2004). Relationship between sediment supply and avulsion frequency in braided rivers. *Geology*, *32*, 21–24.

Ashworth, P. J., Best, J. L., & Jones, M. A. (2007). The relationship between channel avulsion, flow occupancy and aggradation in braided rivers: Insights from an experimental model. *Sedimentology*, *54*, 497–513.

Azzaro, R., Bernardini, F., Camassi, R., & Castelli, V. (2007). The 1780 seismic sequence in NE Sicily (Italy): Shifting an underestimated and mislocated earthquake to a seismically low rate zone. *Natural Hazards*, *42*, 149–167.

Bada, J. L., Belluomini, G., Bonfiglio, L., Branca, M., Burgio, E., & Delitalia, L. (1991). Isoleucin epimerization ages of quaternary mammals from Sicily. *Il Quaternario*, *4*(1), 49–54.

Balescu, S., & Lamothe, M. (1994). Comparison of TL and IRSL age estimates of feldspar coarse grains from waterlain sediments. *Quaternary Science Reviews*, *13*, 437–444.

Baratta, M. (1910). *La catastrofe sismica calabro-messinese (28 Dicembre 1908)*. Relazione alla Società Geografica Italiana.

Barreca, G., Scarfì, L., Gross, F., Monaco, C., & De Guidi, G. (2019). Fault pattern and seismotectonic potential at the south-western edge of the Ionian subduction system (southern Italy): New field and geophysical constraints. *Tectonophysics*, *761*, 31–45.

Barrier, P. (1987). Stratigraphie des dépots pliocènes et quaternaires du Detroit de Messine (Italie). *Documents et travaux de l'IGAL*, *11*, 59–81.

Beaumont, C., Fullsack, P., & Hamilton, J. (1992). Erosional control of active compressional orogens. In K. R. McClay (Ed.), *Thrust tectonics*. Springer. https://doi.org/10.1007/978-94-011-3066-0_1

Billi, A., Barberi, G., Faccenna, C., Neri, G., Pepe, F., & Sulli, A. (2006). Tectonics and seismicity of the Tindari fault system, southern Italy: Crustal deformation at the transition between ongoing contractional and extensional domains located above the edge of a subducting slab. *Tectonics*, *25*, TC2006. https://doi.org/10.1029/2004TC001763

Blair, T. C., & Bilodeau, W. L. (1988). Development of tectonic cyclothems in rift, pull-apart, and foreland basins: Sedimentary response to episodic tectonism. *Geology*, *1988*(16), 517–520. https://doi.org/10.1130/0091-7613(1988)016<0517:DOTCIR>2.3.CO;2

Boccaletti, M., Cello, G., & Tortorici, L. (1990). Strike-slip deformation as a fundamental process during the Neogene-Quaternary evolution of the Tunisian-Pelagian area. *Annales Tectonicae*, *4*, 104–119.

Boersma, J. R., & Terwindt, J. H. J. (1981). Neap-spring tide sequences of intertidal shoal deposits in a mesotidal estuary. *Sedimentology*, *28*, 151–170.

Bonfiglio, L. (1983). Terrazzi marini e depositi continentali quaternari di Taormina. *Quaternaria*, *23*, 81–98.

Bonfiglio, L. (1991). Correlazioni tra depositi a mammiferi, depositi marini, linee di costa e terrazzi medio e tardo-pleistocenici nella Sicilia orientale. *Il Quaternario*, *4*(1b), 205–214.

Bonfiglio, L., & Violanti, D. (1984). Prima segnalazione di Tirreniano ed evoluzione pleistocenica del Capo Peloro (Sicilia nord-orientale). *Geografia Fisica e Dinamica Quaternaria*, *6*(1983), 3–15.

Bonnet, S., & Crave, A. (2003). Landscape response to climate changes: Insights from experimental modeling and implications for tectonic versus climatic uplift of topography. *Geology*, *31*(2), 123–126.

Boschi, E., Guidoboni, E., Ferrari, G., Valensise, G., & Gasperini, P. (1997). *Catalogo dei forti terremoti in Italia dal 461 a.C. al* (p. 1990). Istituto Nazionale di Geofisica. S.G.A.

Bryant, M., Falk, P., & Paola, C. (1995). Experimental-study of avulsion frequency and rate of deposition. *Geology*, *23*, 365–368.

Bull, W. B. (1991). *Geomorphic responses to climate change* (p. 326). Oxford.

Burbank, D. W. (1992). Causes of recent Himalayan uplift deduced from deposited patterns in the Ganges basin. *Nature*, *357*, 680–682.

Cammarata, L., Catalano, S., Gambino, S., Palano, M., Pavano, F., Romagnoli, G., Scaltrito, A., & Tortorici, G. (2018). Seismological and structural constraints on the 2011–2013, Mmax 4.6 seismic sequence at the south-eastern edge of the Calabrian arc (North-eastern Sicily, Italy). *Geomorphology*, *723*, 56–67.

Carbone, S., Messina, A., & Lentini, F. (2008). *Note Illustrative del F. 601 "Messina-Reggio di Calabria" della Carta Geologica d'Italia alla scala 1:50.000. APAT* (p. 179). S.EL.CA.

Cartigny, M. J. B., Ventra, D., Postma, G., & Van den Berg, J. H. (2014). Morphodynamics and sedimentary structures of bedforms under supercritical-flow conditions: New insights from flume experiments. *Sedimentology*, *61*, 712–748.

Castelltort, S., & Van Den Driessche, J. (2003). How plausible are high-frequency sediment supply-driven cycles in the stratigraphic record? *Sedimentary Geology*, *157*, 3–13.

Catalano, S., Cirrincione, R., Mazzoleni, P., Pavano, F., Pezzino, A., Romagnoli, G., & Tortorici, G. (2018). The effects of a Meso-Alpine collision event on the tectono-metamorphic evolution of the Peloritani mountain belt (eastern Sicily, southern Italy). *Geological Magazine*, *155*(2), 422–437.

Catalano, S., & De Guidi, G. (2003). Late Quaternary uplift of north-eastern Sicily: Relation with the active normal faulting deformation. *Journal of Geodynamics*, *36*, 445–467.

Catalano, S., De Guidi, G., Monaco, C., Tortorici, G., & Tortorici, L. (2003). Long-term behavior of the late Quaternary normal faults in the Straits of Messina area (Calabrian arc): Structural and morphological constraints. *Quaternary International*, *101*, 81–91. https://doi.org/10.1016/S1040-6182(02)00091-5

Catalano, S., De Guidi, G., Monaco, C., Tortorici, G., & Tortorici, L. (2008). Active faulting and seismicity along the Siculo-Calabrian rift zone. *Tectonophysics*, *453*, 177–192.

Catalano, S., & Di Stefano, A. (1997). Sollevamento e tettogenesi Pleistocenica lungo il margine tirrenico dei Monti Peloritani: integrazione dei dati geomorfologici, strutturali e biostratigrafici. *Il Quaternario*, *10*, 337–342.

Catuneanu, O., Abreu, V., Bhattacharya, J. P., Blum, M. D., Dalrymple, R. W., Eriksson, P. G., Fielding, C. R., Fisher, W. L.,

13652117, 2024, 1, Downloaded from https://onlinelibrary.wiley.com/doi/10.1111/bre.12845 by Uni Federico II Di Napoli, Wiley Online Library on [17/01/2024]. See the Terms and Conditions (https://onlinelibrary.wiley.com/terms-and-conditions) on Wiley Online Library for rules of use; OA articles are governed by the applicable Creative Commons License

Galloway, W. E., Gibling, M. R., Giles, K. A., Holbrook, J. M., Jordan, R., Kendall, C. G., Macurda, B., Martinsen, O. J., Miall, A. D., Neal, J. E., Nummedal, D., ... Winker, C. (2009). Towards the standardization of sequence stratigraphy. *Earth Science Reviews*, *92*, 1–33.

Cello, G., Guerra, I., Tortorici, L., Turco, E., & Scarpa, R. (1982). Geometry of the neotectonic stress field in southern Italy: Geological and seismological evidence. *Journal of Structural Geology*, *4*, 385–393.

Clarke, L. E., Quine, T. A., & Nicholas, A. P. (2008). An evaluation of the role of physical models in exploring form process feedbacks in alluvial fans. In J. Schmidt, T. Cochrane, C. Phillips, S. Elliott, T. Davies, & L. Basher (Eds.), *Sediment dynamics in changing environments* (pp. 175–183). IAHS Publication 325, Proceedings of a Symposium Held in Christchurch, New Zealand.

Coleman, J. (1975). *Deltas: Processes of deposition and models for exploaration*. Continuing Education.

Comerci, V., Vittori, E., Blumetti, A. M., Brustia, E., Di Manna, P., Guerrieri, L., Lucarini, M., & Serva, L. (2015). Environmental effects of the December 28, 1908, Southern Calabria–Messina (Southern Italy) earthquake. *Natural Hazards*, *76*, 1849–1891. https://doi.org/10.1007/s11069-014-1573-x

Corbett, L. B., Bierman, P. R., & Rood, D. H. (2016). An approach for optimizing in situ cosmogenic ^{10}Be sample preparation. *Quaternary Geochronology*, *33*, 24–34. https://doi.org/10.1016/j.quageo.2016.02.001

Cyr, A. J., Granger, D. E., Olivetti, V., & Molin, P. (2010). Quantifying rock uplift rates using channel steepness and cosmogenic nuclide–determined erosion rates: Examples from northern and southern Italy. *Lithosphere*, *2*(3), 188–198.

Dalrymple, R. W., Baker, E. K., Harris, P. T., & Hughes, M. G. (2003). Sedimentology and stratigraphy of a tide-dominated, foreland-basin delta (Fly River, Papua New Guinea). *Sedimentology, Stratigraphy, and Petroleum Geology Special Publication*, *76*, 147–173.

De Guidi, G., Catalano, S., Monaco, C., & Tortorici, L. (2003). Morphological evidence of Holocene coseismic deformation in the Taormina region (NE Sicily). *Journal of Geodynamics*, *36*, 193–211.

De Guidi, G., Catalano, S., Monaco, C., Tortorici, L., & Di Stefano, A. (2002). Long-term effects of late Quaternary normal faulting in southern Calabria and eastern Sicily. *Studi Geologici Camerti, Nuova Serie*, *1*, 79–93.

De Haas, T., Berg, W., Braat, L., & Kleinhans, M. G. (2016). Autogenic avulsion, channelization and backfilling dynamics of debris-flow fans. *Sedimentology*, *63*, 1596–1619.

Del Ben, A., Gargano, C., & Lentini, R. (1996). Ricostruzione stratigrafica e strutturale dell'area dello Stretto di Messina mediante analisi comparata dei dati geologici e sismici. *Memorie Della Societa'Geologica Italiana*, *51*, 703–717.

Densmore, A. L., Allen, P. A., & Simpson, G. (2007). Development and response of a coupled catchment fan system under changing tectonic and climatic forcing. *Journal of Geophysical Research*, *112*, F01002. https://doi.org/10.1029/2006JF000474

Dewey, J. F., Helman, M. L., Turco, E., Hutton, D. H. W., & Knott, S. D. (1989). Kinematics of the western Mediterranean. In M. P. Coward, R. Gillcrist, & B. Trudgill (Eds.), *Alpine tectonics* (Vol. *45*, pp. 265–283). Geological Society, London, Special Publication. https://doi.org/10.1144/GSL.SP.1989.045.01.15

Di Biase, R. A. (2018). Short communication: Increasing vertical attenuation length of cosmogenic nuclide production on steep slopes negated topographic shielding corrections for catchment erosion rates: Earth Surface. *Dynamics (Pembroke, Ont.)*, *6*, 923–931. https://doi.org/10.5194/esurf-6-923-2018

Di Stefano, A., & Caliri, A. (1996). Dati biostratigrafici sui depositi pleistocenici di Naso (Messina), Sicilia nord-orientale. *Bollettino della Societa Paleontologica Italiana*, *35*(3), 229–238.

Dickinson, W. R., & Suczek, C. A. (1979). Plate tectonics and sandstone composition. *American Association of Petroleum Geologists Bulletin*, *63*, 2164–2172.

Dorsey, R. J., Umhoefe, P. J., & Falk, P. D. (1997). Earthquake clustering inferred from Pliocene Gilbert-type fan deltas in the Loreto Basin, Baja California Sur, Mexico. *Geology*, *25*(8), 679–682.

Dumas, S., & Arnott, R. C. W. (2006). Origin of hummocky and swaley cross-stratification. The controlling influence of unidirectional current strength and aggradation rate. *Geology*, *34*, 1073–1076.

Durcan, J. A., King, G. E., & Duller, G. A. T. (2015). DRAC: Dose rate and age calculator for trapped charge dating. *Quaternary Geochronology*, *28*, 54–61.

Ettensohn, F. R., Lierman, R. T., Udgata, D. B. P., & Mason, C. E. (2012). The Early-Middle Mississippian Borden–Grainger–Fort Payne delta/basin complex: Field evidence for delta sedimentation, basin starvation, mud-mound genesis, and tectonism during the Neoacadian Orogeny. In M. C. Eppes & M. J. Bartholomew (Eds.), *From the blue ridge to the coastal plain: Field excursions in the southeastern United States* (Vol. *29*, pp. 345–395). Geological Society of America Field Guide. https://doi.org/10.1130/2012.0029(11)

Faccenna, C., Molin, P., Orecchio, B., Olivetti, V., Bellier, O., & Funiciello, F. (2011). Topography of the Calabria subduction zone (southern Italy): Clues for the origin of Mt. Etna. *Tectonics*, *30*, TC1003.

Faccenna, C., Piromallo, C., Crespo-Blanc, A., Jolivet, L., & Rossetti, F. (2004). Lateral slab deformation and the origin of the western Mediterranean arcs. *Tectonics*, *23*, TC1012. https://doi.org/10.1029/2002TC001488

Feng, W.-J., Zhang, C.-M., Yin, T.-J., Yin, Y.-S., Liu, J.-L., Zhu, R., Xu, Q.-H., & Chen, Z. (2019). Sedimentary characteristics and internal architecture of a river-dominated delta controlled by autogenic process: Implications from a flume tank experiment. *Petroleum Science*, *16*, 1237–1254. https://doi.org/10.1007/s12182-019-00389-x

Ferranti, L., Antonioli, F., Anzidei, M., Monaco, C., & Stocchi, P. (2010). The timescale and spatial extent of recent vertical tectonic motions in Italy: Insights from relative sea-level changes studies. *Journal of the Virtual Explorer*, *36*, 23. https://doi.org/10.3809/jvirtex.2010.00255

Fisher, J. A., Pazzaglia, F. J., Anastasio, D. J., & Gallen, S. F. (2022). Linear inversion of fluvial topography in the northern Apennines: Comparison of base-level fall to crustal shortening. *Tectonics*, *41*, e2022TC007379. https://doi.org/10.1029/2022TC007379

Foreman, B. Z., & Straub, K. M. (2017). Autogenic geomorphic processes determine the resolution and fidelity of terrestrial paleoclimate records. *Science Advances*, *3*(9), e1700683. https://doi.org/10.1126/sciadv.1700683

Forte, A. M., & Whipple, K. X. (2019). Short communication: The Topographic Analysis Kit (TAK) for TopoToolbox. *Earth Surface Dynamics*, *7*, 87–95. https://doi.org/10.5194/esurf-7-87-2019

13652117, 2024, 1, Downloaded from https://onlinelibrary.wiley.com/doi/10.1111/bre.12845 by Uni Federico II Di Napoli, Wiley Online Library on [17/01/2024]. See the Terms and Conditions (https://onlinelibrary.wiley.com/terms-and-conditions) on Wiley Online Library for rules of use; OA articles are governed by the applicable Creative Commons License

Forzoni, A., Storms, J. E. A., Whittaker, A. C., & De Jager, G. (2014). Delayed delivery from the sediment factory: Modeling the impact of catchment response time to tectonics on sediment flux and fluvio-deltaic stratigraphy. *Earth Surface Processes and Landforms*, *39*, 689–704.

Foti, A., Pavano, F., Romagnoli, G., Tortorici, G., & Catalano, S. (2023). Structural geology of the eastern termination of the Mt. Kumeta-Alcantara line (NE sicily, Italy). *Journal of Maps*, *19*(1), 2179436. https://doi.org/10.1080/17445647.2023.2179436

Gallen, S. F. (2018). Lithologic controls on landscape dynamics and aquatic species evolution in post-orogenic mountains. *Earth and Planetary Science Letters*, *493*, 150–160. https://doi.org/10.1016/j.epsl.2018.04.029

Gallen, S. F., & Fernández-Blanco, D. (2021). A new data-driven Bayesian inversion of fluvial topography clarifies the tectonic history of the corinth rift and reveals a channel steepness threshold. *Journal of Geophysical Research: Earth Surface*, *126*, e2020JF005651. https://doi.org/10.1029/2020JF005651

Galloway, W. (1975). In M. Broussard (Ed.), *Process framework for describing the morphologic and stratigraphic evolution of deltaic depositional systems* (pp. 87–98). Houston Geological Society.

Ganti, V., Chadwick, A., Hassenruck-Gudipati, H., Fuller, B., & Lamb, M. (2016). Experimental river delta size set by multiple floods and backwater hydrodynamics. *Science Advances*, *2*, e1501768. https://doi.org/10.1126/sciadv.1501768

Ganti, V., Chu, Z., Lamb, M. P., Nittrouer, J. A., & Parker, G. (2014). Testing morphodynamic controls on the location and frequency of river avulsions on fans versus deltas: Huanghe (Yellow River), China. *Geophysical Research Letters*, *41*, 7882–7890. https://doi.org/10.1002/2014GL061918

Giammanco, S., Palano, M., Scaltrito, A., Scarfì, L., & Sortino, F. (2008). Possible role of fluid overpressure in the generation of earthquake swarms in active tectonic areas: The case of the Peloritani Mts. (Sicily, Italy). *Journal of Volcanology and Geothermal Research*, *178*(4), 795–806.

Godard, V., Tucker, G. E., Burch Fisher, G., Burbank, D. W., & Bookhagen, B. (2013). Frequency-dependent landscape response to climatic forcing. *Geophysical Research Letters*, *40*(5), 859–863.

Goren, L., Fox, M., & Willett, S. D. (2014). Tectonics from fluvial topography using formal linear inversion: Theory and applications to the Inyo Mountains, California. *Journal of Geophysical Research: Earth Surface*, *119*(8), 1651–1681. https://doi.org/10.1002/2014JF003079

Guérin, G., Mercier, N., & Adamiec, G. (2011). Dose-rate conversion factors: Update. *Ancient TL*, *29*, 5–8.

Hancock, G. S., Anderson, R. S., & Whipple, K. X. (1998). Beyond power: Bedrock river incision process and form. In K. J. Tinkler & E. E. Wohl (Eds.), *Rivers over rock: Fluvial processes in bedrock channels* (Vol. *107*, pp. 35–60). American Geophysical Union Geophysical Monograph. https://doi.org/10.1029/GM107p0035

Harms, J. C., Southard, J. B., Spearing, D. R., & Walker, R. G. (1975). *Depositional environments as interpreted from primary sedimentary structures and stratification sequences*. SEPM Short Course, n. 2.

Hoffman, P. F., & Grotzinger, J. P. (1993). Orographic precipitation, erosional unloading, and tectonic style. *Geology*, *21*(3), 195–198.

Howard, A. D. (1994). A detachment-limited model of drainage basin evolution. *Water Resources Research*, *30*(7), 2261–2285.

Huntley, D. J., & Baril, M. R. (1997). The K content of the K-feldspars being measured in optical dating or in the thermoluminescence dating. *Ancient TL*, *15*(1), 11–13.

Huntley, D. J., & Hancock, R. G. V. (2001). The Rb contents of the K-feldspar grains being measured in optical dating. *Ancient TL*, *19*(2), 43–46.

Jerolmack, D. J., & Paola, C. (2010). Shredding of environmental signals by sediment transport. *Geophysical Research Letters*, *37*, L19401. https://doi.org/10.1029/2010GL044638

Jerolmack, D. J., & Sadler, P. (2007). Transience and persistence in the depositional record of continental margins. *Journal of Geophysical Research*, *112*, F03S13. https://doi.org/10.1029/2006JF000555

Kastens, K. A., Mascle, J., Auroux, C., Bonatti, E., Broglia, C., Channell, J. E. T., Curzi, P., Emeis, K. C., Glaçon, G., Hasegawa, S., & Hieke, W. (1988). ODP leg 107 in the Tyrrhenian Sea: Insights into passive margin and backarc basin evolution. *Geological Society of America Bulletin*, *100*, 1140–1156.

Kim, W., & Jerolmack, D. J. (2008). The pulse of calm fan deltas. *Journal of Geology*, *116*, 315–330.

Kim, W., & Paola, C. (2007). Long-period cyclic sedimentation with constant tectonic forcing in an experimental relay ramp. *Geology*, *35*(4), 331–334.

Kim, W., Paola, C., Swenson, J. B., & Voller, V. R. (2006). Shoreline response to autogenic processes of sediment storage and release in the fluvial system. *Journal of Geophysical Research—Earth Surface*, *111*, F04013. https://doi.org/10.1029/2006JF000470

Kirby, E., & Whipple, K. X. (2012). Expression of active tectonics in erosional landscapes. *Journal of Structural Geology*, *44*, 54–75. https://doi.org/10.1016/j.jsg.2012.07.009

Kohl, C., & Nishiizumi, K. (1992). Chemical isolation of quartz for measurement of in-situ-produced cosmogenic nuclides. *Geochimica et Cosmochimica Acta*, *56*, 3583–3587.

Koons, P. O. (1989). The topographic evolution of collisional mountain belts: A numerical look at the southern Alps, New Zealand. *American Journal of Science*, *289*, 1041–1069.

Lague, D. (2013). The stream power river incision model: Evidence, theory and beyond. *Earth Surface Processes and Landforms*, *39*, 38–61.

Lamothe, M., Auclair, M., Hamzaoi, C., & Huot, S. (2003). Towards a prediction of long-term anomalous fading of feldspar IRSL. *Radiation Measurements*, *37*(4–5), 493–498. https://doi.org/10.1016/S1350-4487(03)00016-7

Lang, J., & Winsemann, J. (2013). Lateral and vertical facies relationships of bedforms deposited by aggrading supercritical flows: From cyclic steps to humpback dunes. *Sedimentary Geology*, *296*, 36–54.

Leeder, M. R., & Jackson, J. A. (1993). The interaction between normal faulting and drainage in active extensional basins, with examples from the western United States and Central Greece. *Basin Research*, *5*, 79–102.

Lentini, F., Carbone, S., Catalano, S., & Grasso, M. (1995). Principali lineamenti strutturali della Sicilia nord-orientale. *Studi Geologici Camerti*, *2*, 319–329.

Lentini, F., Catalano, S., & Carbone, S. (2000). *Note illustrative della Carta geologica della Provincia di Messina, scala 1:50.000*. Con il contributo di Di Sefano, A., Messina, A., Romeo, M. and Vinci G. (p. 70). S.EL.CA.

Lentini, F., & Vezzani, L. (1975). Le unità meso-cenozoiche della copertura sedimentaria del basamento cristallino peloritano

13652117, 2024, 1, Downloaded from https://onlinelibrary.wiley.com/doi/10.1111/bre.12845 by Uni Federico II Di Napoli, Wiley Online Library on [17/01/2024]. See the Terms and Conditions (https://onlinelibrary.wiley.com/terms-and-conditions) on Wiley Online Library for rules of use; OA articles are governed by the applicable Creative Commons License

(Sicilia nord-orientale). *Bollettino della Societa Geologica Italiana*, *94*(3), 537–554.

Li, Q., Gasparini, N. M., & Straub, K. M. (2018). Some signal are not the same as they appear: How do erosional landscape transform tectonic history into sediment flux records? *Geology*, *46*(5), 407–410.

Lisiecki, L. E., & Raymo, M. E. (2005). A Pliocene-Pleistocene stack of 57 globally distributed benthic d^{18}O records. *Paleoceanography*, *20*, PA1003. https://doi.org/10.1029/2004PA001071

Longhitano, S. G. (2018). Between Scylla and Charybdis (part 1): The sedimentary dynamics of the modern Messina Strait (Central Mediterranean) as analogue to interpret the past. *Earth-Science Reviews*, *185*, 259–287.

Malinverno, A. (2012). Evolution of the Tyrrhenian Sea-Calabrian arc system: The past and the present. *Rendiconti Online della Società Geologica Italiana*, *21*, 11–15.

Malinverno, A., & Ryan, W. B. F. (1986). Extension in the Tyrrhenian Sea and shortening in the Apennines as a result of arc migration driven by sinking of the lithosphere. *Tectonics*, *5*, 227–245. https://doi.org/10.1029/TC005i002p00227

Mastrolembo Ventura, B., Serpelloni, E., Argnani, A., Bonforte, A., Bürgmann, R., Anzidei, M., Baldi, P., & Puglisi, G. (2014). Fast geodetic strain-rates in eastern Sicily (southern Italy): New insights into block tectonics and seismic potential in the area of the great 1693 earthquake. *Earth and Planetary Science Letters*, *404*, 77–88. https://doi.org/10.1016/j.epsl.2014.07.025

Matenco, L. C., & Haq, B. U. (2020). Multi-scale depositional successions in tectonic settings. *Earth-Science Reviews*, *200*, 102991. https://doi.org/10.1016/j.earscirev.2019.102991

Mejdahl, V. (1979). Thermoluminescence dating: Beta-dose attenuation in quartz grains. *Archaeometry*, *21*, 61–72.

Meschis, M., Roberts, G. P., Mildon, Z. K., Robertson, J., Michetti, A. M., & Faure Walker, J. P. (2019). Slip on a mapped normal fault for the 28th December 1908 Messina earthquake (mw 7.1) in Italy. *Scientific Reports*, *9*(1), 6481. https://doi.org/10.1038/s41598-019-42915-2

Meschis, M., Roberts, G. P., Robertson, J., & Briant, R. M. (2018). The relationships between regional quaternary uplift, deformation across active normal faults, and historical seismicity in the upper plate of subduction zones: The capo D'Orlando fault, NE Sicily. *Tectonics*, *37*, 1231–1255. https://doi.org/10.1029/2017TC004705

Miall, A. D. (1997). *The geology of stratigraphic sequences* (p. 433). Springer.

Monaco, C., & Tortorici, L. (2000). Active faulting in the Calabrian arc and eastern Sicily. *Journal of Geodynamics*, *29*, 407–424.

Montgomery, D. R., & Foufoula-Georgiou, E. (1993). Channel network source representation using digital elevation models. *Water Resources Research*, *29*, 3925–3934. https://doi.org/10.1029/93WR02463

Mutti, E., Allen, G. P., & Rossel, J. (1984). *Sigmoidal-cross stratification and sigmoidal bars: Depositional features diagnostic of tidal sandstones*. 5th IAS European Regional Meeting, Marsiglia, Abstract volume, 312–313.

Mutti, E., Rossel, J., Allen, G. P., Fonnesu, F., & Sgavetti, M. (1985). The Eocene Baronia tide dominated delta-shelf system in the Ager Basin. In M. Mila & J. Rosell (Eds.), *6th IAS European Regional Meeting, Field Trip Guide Book* (pp. 579–600).

Mutti, E., Tinterri, R., Di Biase, D., Fava, L., Mavilla, N., Angella, S., & Calabrese, L. (2000). Delta-front facies associations of ancient flood-dominated fluvio-deltaic systems. *Revista de la Sociedad Geológica de España*, *13*, 165–190.

Nelson, M., Rittenour, T., & Cornachione, H. (2019). Sampling methods for luminescence dating of subsurface deposits from cores. *Methods and Protocols*, *2*(4), 88. https://doi.org/10.3390/mps2040088

Nelson, M. S., Gray, H. J., Johnson, J. A., Rittenour, T. M., Feathers, J. K., & Mahan, S. A. (2015). User guide for luminescence sampling in archaeological and geological contexts. *Advances in Archaeological Practice*, *3*(2), 166–177.

Neri, G., Oliva, G., Orecchio, B., & Presti, D. (2006). A possible seismic gap within a highly seismogenic belt crossing Calabria and Eastern Sicily, Italy. *Bulletin of the Seismological Society of America*, *96*, 1321–1331.

Nicholas, A. P., & Quine, T. A. (2007). Modeling alluvial landform change in the absence of external environmental forcing. *Geology*, *35*, 527–530.

Nishiizumi, K., Imamura, M., Caffee, M. W., Southon, J. R., Finkel, R. C., & McAninch, J. (2007). Absolute calibration of ^{10}Be AMS standards. *Nuclear Instruments and Methods in Physics Research Section B: Beam Interactions with Materials and Atoms*, *258*, 403–413.

Olsen, P. E., Withjack M., Schlische R. W., & Pazzaglia F. J. (2018). *Temporal, tectonic, climatic and environmental context of the Triassic-Jurassic rift system of eastern North America: Emerging concepts from the Newark rift basin*. Field Trip Guidebook. Field Conference of Pennsylvania Geologists Center Valley, PA October 5–6, 2018.

Ott, R. F., Scherler, D., Wegmann, K. W., D'Arcy, M. K., Pope, R. J., Ivy-Ochs, S., Christi, M., Vockenhuber, C., & Rittenour, T. M. (2022). Paleo-denudation rates suggest variations in runoff drove aggradation during last glacial cycle, Crete, Greece. *Earth Surface Processes and Landforms*, *48*, 386–405.

Paola, C. (2000). Quantitative models of sedimentary basin filling. *Sedimentology*, *47*(Suppl. 1), 121–178.

Paola, C., Ganti, V., Mohrig, D., Runkel, A. C., & Straub, K. M. (2018). Time not our time: Physical controls on the preservation and measurement of geologic time. *Annual Review of Earth and Planetary Sciences*, *46*, 409–438.

Paola, C., Heller, P. L., & Angevine, C. L. (1992). The large-scale dynamics of grain size variation in alluvial basins. 1, theory. *Basin Research*, *4*, 73–90.

Paola, C., Mullin, J., Ellis, C., Mohrig, D. C., Swenson, J. B., Parker, G., Hickson, T., Heller, P. L., Pratson, L., Syvitski, J., Sheets, B., & Strong, N. (2001). Experimental stratigraphy. *GSA Today*, *11*(7), 4–9. https://doi.org/10.1130/1052-5173(2001)011<0004:ES>2.0.CO;2

Pavano, F., Catalano, S., Romagnoli, G., & Tortorici, G. (2018). Hypsometry and relief analysis of the southern termination of the Calabrian arc, NE-Sicily (southern Italy). *Geomorphology*, *304*, 74–88.

Pavano, F., & Gallen, S. F. (2021). A geomorphic examination of the Calabrian Forearc translation. *Tectonics*, *40*, e2020TC006692. https://doi.org/10.1029/2020TC006692

Pavano, F., Pazzaglia, F. J., & Catalano, S. (2016). Knickpoints as geomorphic markers of active tectonics: A case study from northeastern Sicily (southern Italy). *Lithosphere*, *8*(6), 633–648. https://doi.org/10.1130/L577.1

Pavano, F., Romagnoli, G., Tortorici, G., & Catalano, S. (2015). Active tectonics along the Nebrodi–Peloritani boundary in

13652117, 2024, 1, Downloaded from https://onlinelibrary.wiley.com/doi/10.1111/bre.12845 by Uni Federico II Di Napoli, Wiley Online Library on [17/01/2024]. See the Terms and Conditions (https://onlinelibrary.wiley.com/terms-and-conditions) on Wiley Online Library for rules of use; OA articles are governed by the applicable Creative Commons License

northeastern Sicily (southern Italy). *Tectonophysics*, *659*, 1–11. https://doi.org/10.1016/j.tecto.2015.07.024

Pazzaglia, F. J., & Fisher, J. (2022). A reconstruction of Apennine uplift history and the development of transverse drainages from longitudinal profile inversion. In C. Koeberl, P. Claeys, & S. Montanari (Eds.), *From the Guajira desert to the Apennines, and from Mediterranean microplates to the Mexican killer asteroid*. Geological Society of America Special Papers, 557.

Pezzino, A., Angi, G., Cirrincione, R., De Vuono, E., Fazio, E., Fiannacca, P., Lo, G. A., Ortolano, G., & Punturo, R. (2008). Alpine metamorphism in the Aspromonte Massif: Implications for a new framework for the southern sector of the Calabria-Peloritani Orogen (Italy). *International Geology Review*, *50*, 423–441.

Pizzuto, J., Keeler, J., Skalak, K., & Karwan, D. (2017). Storage filters upland suspended sediment signals delivered from watersheds. *Geology*, *4*(2), 151–154.

Playfair, J. (1802). *Illustrations of the Huttonian theory of the Earth*. Cadell and Davies.

Postma, G., Hoyal, D. C., Demko, T., Fedele, J. J., Lang, J., Abreu, V., & Pederson, K. H. (2020). Reconstruction of bedform dynamics controlled by supercritical flow in the channel–lobe transition zone of adeep-water delta (Sant Llorencßdel Munt, north-east Spain, Eocene). *Sedimentology*, *68*, 1674–1697. https://doi.org/10.1111/sed.12735

Postpischl, D. (1985). *Catalogo dei terremoti italiani dall'anno 1000 al 1980* (p. 239). CNR, P.F. Geodinamica, Graficoop Bologna.

Prescott, J. R., & Hutton, J. T. (1994). Cosmic ray contributions to dose rates for luminescence and ESR dating. *Radiation Measurements*, *23*, 497–500.

Rittenour, T. M. (2018). Dates and rates of Earth-surface processes revealed using luminescence dating. *Elements*, *14*, 21–26.

Riuscetti, M., & Shick, R. (1975). Earthquakes and tectonics in Southern Italy. *Bollettino di Geofisica Teorica ed Applicata*, *17*, 58–78.

Rohais, S., Bonnet, S., & Eschard, R. (2012). Sedimentary record of tectonic and climatic erosional perturbations in an experimental coupled catchment-fan system. *Basin Research*, *24*, 198–212.

Romans, B. W., Castelltort, S., Covault, J. A., Fildani, A., & Walsh, J. P. (2015). Environmental signal propagation in sedimentary systems across timescales. *Earth Science Reviews*, *153*, 7–29. https://doi.org/10.1016/j.earscirev.2015.07.012

Rosenbaum, G., & Lister, G. S. (2004). Neogene and Quaternary rollback evolution of the Tyrrhenian Sea, the Apennines, and the Sicilian Maghrebides. *Tectonics*, *23*, TC1013. https://doi.org/10.1029/2003TC001518

Rovida, A., Locati, M., Camassi, R., Lolli, B., Gasperini, P., & Antonucci, A. (2022). *Catalogo Parametrico dei Terremoti Italiani (CPTI15), versione 4.0*. Istituto Nazionale di Geofisica e Vulcanologia (INGV). https://doi.org/10.13127/CPTI/CPTI15.4

Rust, D., & Kershaw, S. (2000). Holocene tectonic uplift patterns in northeastern Sicily evidence from marine notches in coastal outcrops. *Marine Geology*, *167*, 105–126.

Scarfì, L., Barberi, G., Musumeci, C., & Patanè, D. (2016). Seismotectonics of northeastern Sicily and southern Calabria (Italy): New constraints on the tectonic structures featuring in a crucial sector for the central Mediterranean geodynamics. *Tectonics*, *35*, 812–832. https://doi.org/10.1002/2015TC004022

Schumer, R., Jerolmack, D. J., & McElroy, B. (2011). The stratigraphic filter and bias in measurement of geologic rates. *Geophysical Research Letters*, *38*(11), L11405. https://doi.org/10.1029/2011GL047118

Schumm, S. A., Mosley, P. M., & Weaver, P. H. (1987). *Experimental fluvial geomorphology* (p. 413). John Wiley & Sons.

Schumm, S. A., & Rea, D. K. (1995). Sediment yield from disturbed earth systems. *Geology*, *23*, 391–394.

Schwanghart, W., & Scherler, D. (2014). Short Communication: TopoToolbox 2—MATLAB-based software for topographic analysis and modelling in Earth surface sciences. *Earth Surface Dynamics*, *2*, 1–7. https://doi.org/10.5194/esurf-2-1-2014

Schwanghart, W., & Scherler, D. (2017). Bumps in river profiles: Uncertainty assessment and smoothing using quantile regression techniques. *Earth Surface Dynamics*, *5*, 821–839. https://doi.org/10.5194/esurf-5-821-2017

Selli, R. (1978). Geologia e sismotettonica dello Stretto di Messina. Convegno: "L'attraversamento dello Stretto di Messina e la sua fattibilità", 4–6 Luglio 1978. *Atti della Accademia Nazionale dei Lincei*, *43*, 119–154.

Serpelloni, E., Vannucci, G., Pondrelli, S., Argnani, A., Casula, G., Anzidei, M., Baldi, P., & Gasperini, I. (2007). Kinematics of the western Africa–Eurasia plate boundary from focal mechanisms and GPS data. *Geophysical Journal International*, *169*, 1180–1200. https://doi.org/10.1111/j.1365-246X.2007.03367.x

Seybold, H., Andrade, J. S., Jr., & Herrmann, H. J. (2007). Modeling river delta formation. *Proceedings of the National Academy of Sciences of the United States of America*, *104*(43), 16804–16809.

Sharman, G. R., Sylvester, Z., & Covault, J. A. (2019). Conversion of tectonic and climatic forcings into records of sediment supply and provenance. *Scientific Reports*, *9*, 4115. https://doi.org/10.1038/s41598-019-39754-6

Simpson, G., & Castelltort, S. (2012). Model shows that rivers transmit high-frequency climate cycles to the sedimentary record. *Geology*, *40*, 1131–1134. https://doi.org/10.1130/G33451.1

Slingerland, R. (1990). Predictability and chaos in quantitative dynamic stratigraphy. In T. A. Cross (Ed.), *Quantitative dynamic stratigraphy* (pp. 45–53). Prentice-Hall.

Smith, G. A. (1994). Climatic influences on continental deposition during late-stage filling of an extensional basin, southeastern Arizona. *Geological Society of America Bulletin*, *106*, 1212–1228. https://doi.org/10.1130/0016-7606(1994)106<1212:CIOCDD>2.3.CO;2

Snyder, N. P., Whipple, K. X., Tucker, G. E., & Merritts, D. J. (2000). Landscape response to tectonic forcing: Digital elevation model analysis of stream profiles in the Mendocino triple junction region, northern California. *Geological Society of America Bulletin*, *112*, 1250–1263. https://doi.org/10.1130/0016-7606(2000)112<1250:LRTTFD>2.0

Snyder, N. P., Whipple, K. X., Tucker, G. E., & Merritts, D. J. (2002). Interactions between onshore bedrock-channel incision and nearshore wave-base erosion forced by eustasy and tectonics. *Basin Research*, *14*(2), 105–127.

Straub, K. M., Paola, C., Mohrig, D., Wolinsky, M. A., & George, T. (2009). Compensational stacking of channelized sedimentary deposits. *Journal of Sedimentary Research*, *79*(9), 673–688. https://doi.org/10.2110/jsr.2009.070

Tinterri, R. (2011). Combined flow sedimentary structures and the genetic link between sigmoidal- and hummocky-cross stratification. *GeoActa*, *10*, 43–85.

13652117, 2024, 1, Downloaded from https://onlinelibrary.wiley.com/doi/10.1111/bre.12845 by Uni Federico II Di Napoli, Wiley Online Library on [17/01/2024]. See the Terms and Conditions (https://onlinelibrary.wiley.com/terms-and-conditions) on Wiley Online Library for rules of use; OA articles are governed by the applicable Creative Commons License

Tinti, S., Maramai, A., & Graziani, L. (2004). The new catalogue of Italian tsunamis. *Natural Hazards*, *33*, 439–465.

Trampush, S. M., Hajek, E. A., Straub, K. M., & Chamberlin, E. P. (2017). Identifying autogenic sedimentation in fluvial-deltaic stratigraphy: Evaluating the effect of outcrop-quality data on the compensation statistic. *Journal of Geophysical Research—Earth Surface*, *122*, 91–113. https://doi.org/10.1002/2016JF004067

Tucker, G., & Slingerland, R. (1997). Drainage basin responses to climate change. *Water Resources Research*, *33*, 2031–2047. https://doi.org/10.1029/97WR00409

Vail, P. R., Todd, R. G., & Sangree, J. B. (1977). Seismic stratigraphy and global changes of sea level: Part 5. Chronostratigraphic significance of seismic reflections, in application of seismic reflection configuration to stratigraphic interpretation. *AAPG Memorial*, *26*, 99–116.

Valensise, G., & Pantosti, D. (1992). A 125 Kyr-long geological record of seismic source repeatability: The Messina Straits (southern Italy) and the 1908 earthquake (Ms 71/2). *Terra Nova*, *4*, 472–483.

Van Dijk, M., Postma, G., & Kleinhans, M. G. (2009). Autocyclic behavior of fan deltas: An analogue experimental study. *Sedimentology*, *56*(5), 1569–1589. https://doi.org/10.1111/j.1365-3091.2008.01047.x

Waelbroeck, C., Labeyrie, L., Michel, E., Duplessy, J. C., McManus, J. F., Lambeck, K., Balbon, E., & Labracherie, M. (2002). Sea-level and deep water temperature changes derived from benthic foraminifera isotopic records. *Quaternary Science Reviews*, *21*, 295–305.

Wallinga, J., Murray, A., & Wintle, A. G. (2000). The single-aliquot regenerative-dose (SAR) protocol applied to coarse-grain feldspar. *Radiation Measurements*, *32*, 529–533.

Whipple, K. X., Parker, G., Paola, C., & Mohrig, D. (1998). Channel dynamics, sediment transport, and the slope of alluvial fans: Experimental study. *Journal of Geology*, *106*, 677–693.

Whipple, K. X., & Tucker, G. E. (1999). Dynamics of the stream power river incision model: Implications for height limits of mountain ranges, landscape response timescales and research needs. *Journal of Geophysical Research*, *104*(17), 661–717. https://doi.org/10.1029/1999JB900120

Wobus, C., Whipple, X. K., Kirby, E., Snyder, N., Johnson, J., Spyropolou, K., Crosby, B., & Sheehan, D. (2006). Tectonics from topography: Procedures, promise, and pitfalls. In S. D. Willett, N. Hovius, M. T. Brandon, & D. M. Fisher (Eds.), *Tectonics, climate, and landscape evolution* (pp. 55–74. Penrose Conference Series). Geologica Society of America Special Paper 398. https://doi.org/10.1130/2006.2398(04)

Zeitler, P. K., Meltzer, A. S., Koons, P. O., Craw, D., Hallet, B., Chamberlain, C. P., Kidd, W. S. F., Park, S. K., Seeber, L., Bishop, M., & Shroder, J. (2001). Erosion, Himalayan geodynamics, and the geomorphology of metamorphism. *GSA Today*, *11*(1), 4–9.

SUPPORTING INFORMATION

Additional supporting information can be found online in the Supporting Information section at the end of this article.

How to cite this article: Pavano, F., Pazzaglia, F. J., Rittenour, T. M., Catalano, S., Corbett, L. B., & Bierman, P. (2024). Integrated uplift, subsidence, erosion and deposition in a tightly coupled source-to-sink system, Pagliara basin, northeastern Sicily, Italy. *Basin Research*, *36*, e12845. https://doi.org/10.1111/bre.12845

13652117, 2024, 1, Downloaded from https://onlinelibrary.wiley.com/doi/10.1111/bre.12845 by Uni Federico II Di Napoli, Wiley Online Library on [17/01/2024]. See the Terms and Conditions (https://onlinelibrary.wiley.com/terms-and-conditions) on Wiley Online Library for rules of use; OA articles are governed by the applicable Creative Commons License